[redacted]

~~CONFIDENTIAL~~

NASA TECHNICAL MEMORANDUM

NASA TM X-3149

NASA TM X-3149

~~CONFIDENTIAL CLASSIFIED~~
~~BY Security Classification Officer NASA LaRC~~
~~SUBJECT TO GENERAL DECLASSIFICATION SCHEDULE OF EXECUTIVE ORDER 11652 AUTOMATICALLY DOWNGRADED AT TWO YEAR INTERVALS AND DECLASSIFIED ON DEC 31 1980~~

DOWNGRADED TO unclassified
BY AUTHORITY OF NASA CLASSIFICATION
CHANGE NOTICES NO 240 DATED 30 Sep 76
ITEM NO. 55

LOW-SPEED AERODYNAMIC CHARACTERISTICS OF A TRANSPORT CONFIGURATION HAVING A 42° SWEPT SUPERCRITICAL AIRFOIL WING AND THREE TAIL HEIGHT POSITIONS [redacted]

by Paul G. Fournier and William C. Sleeman, Jr.

Langley Research Center
Hampton, Va. 23665

NATIONAL AERONAUTICS AND SPACE ADMINISTRATION • WASHINGTON, D. C. • DECEMBER 1974

~~CONFIDENTIAL~~

[redacted]

1. Report No. NASA TM X-3149	2. Government Accession No.	3. Recipient's Catalog No.

4. Title and Subtitle LOW-SPEED AERODYNAMIC CHARACTERISTICS OF A TRANSPORT CONFIGURATION HAVING A 42^{o} SWEPT SUPERCRITICAL AIRFOIL WING AND THREE TAIL HEIGHT POSITIONS (U)	5. Report Date December 1974 6. Performing Organization Code
7. Author(s) Paul G. Fournier and William C. Sleeman, Jr.	8. Performing Organization Report No. L-9852
9. Performing Organization Name and Address NASA Langley Research Center Hampton, Va. 23665	10. Work Unit No. 505-11-11-01 11. Contract or Grant No.
12. Sponsoring Agency Name and Address National Aeronautics and Space Administration Washington, D.C. 20546	13. Type of Report and Period Covered Technical Memorandum 14. Sponsoring Agency Code

15. Supplementary Notes

16. Abstract

A low-speed investigation was conducted in the Langley V/STOL tunnel to define the static stability characteristics of an advanced high subsonic speed transport aircraft model in the cruise configuration (no high-lift system). The wing of the model had 42^{o} sweep of the quarter-chord line, an aspect ratio of 6.78, and supercritical airfoil sections. Three different horizontal-tail configurations (high, mid, and low) were investigated on the complete model and for the model with the wing removed in order to assess effects of the wing flow field on the tail contributions to both longitudinal and lateral stability characteristics. All the model configurations investigated were tested over an angle-of-attack range from approximately -5^{o} to 23^{o}. Some model configurations were also tested over an angle-of-attack range from about 11^{o} to 38^{o} in order to explore the aerodynamic characteristics in the deep-stall region.

CLASSIFICATION CHANGE

To UNCLASSIFIED
By authority of NASA TD 77-163
Changed by O. Weathe... Date 6/15/76
Classified Document Master Control Station, NASA
Scientific and Technical Information Facility

17. Key Words (Suggested by Author(s))
Supercritical wing
Low-speed aerodynamic characteristics
Swept wing
Tail height
Transport

19. Security Classif. (of this report) [redacted]	20. Security Clas Uncla

[redacted]

LOW-SPEED AERODYNAMIC CHARACTERISTICS OF A TRANSPORT CONFIGURATION HAVING A 42° SWEPT SUPERCRITICAL AIRFOIL WING AND THREE TAIL HEIGHT POSITIONS*

By Paul G. Fournier and William C. Sleeman, Jr.
Langley Research Center

SUMMARY

A low-speed investigation was conducted in the Langley V/STOL tunnel to define the static stability characteristics of an advanced high subsonic speed transport aircraft model in the cruise configuration (no high-lift system). The wing of the model had 42° sweep of the quarter-chord line, an aspect ratio of 6.78, and supercritical airfoil sections. Three different horizontal-tail configurations (high, mid, and low) were investigated on the complete model and for the model with the wing removed in order to assess effects of the wing flow field on the tail contributions to both longitudinal and lateral stability characteristics. All the model configurations investigated were tested over an angle-of-attack range from approximately -5° to 23°. Some model configurations were also tested over an angle-of-attack range from about 11° to 38° in order to explore the aerodynamic characteristics in the deep-stall region.

The test results indicated that both the static longitudinal and lateral aerodynamic characteristics of the model were dominated by the development of unfavorable flow over the wing at moderate to high angles of attack. Wing-body pitching moments became more unstable as the angle of attack increased from 0° up to about 15°. With all the horizontal-tail configurations investigated, the model became longitudinally unstable for angles of attack above about 10°. Static lateral-stability derivatives of the model indicated positive effective dihedral throughout the angle-of-attack range of the investigation. Positive static-directional stability was indicated at low and moderate angles of attack with the vertical tails on, for all horizontal-tail configurations tested. However, the tail contribution generally decreased as the angle of attack increased, and directional instability occurred for angles of attack above 24° with the low horizontal tail.

---

*[redacted]

INTRODUCTION

The National Aeronautics and Space Administration has sponsored a continuing research and technology effort to develop aerodynamic configurations applicable to advanced subsonic commercial transports. Wind-tunnel research conducted at high subsonic speeds (refs. 1 to 3) has shown that the drag rise could be delayed to Mach numbers near unity by the use of supercritical airfoil sections and by proper integration of the wing, engines, and tail surfaces with an area-ruled fuselage. Research has also been conducted at low speeds to develop high-lift systems for supercritical airfoils (ref. 4) and to assess the static stability and high-lift performance of a general research model that simulated an advanced transport configuration (ref. 5).

The present investigation was conducted to define the low-speed static stability characteristics of the clean configuration (no high-lift system) that was developed in the high-speed tests of reference 3. The present model had provisions for varying the vertical location of the horizontal tails. The wing of the model had 42° sweep of the quarter-chord line, an aspect ratio of 6.78, and supercritical airfoil sections. The wing had a large glove that extended from the fuselage outboard to the 32-percent semispan station. The fuselage was contoured for the proper cross-sectional area to account for both the wing glove and the twin nacelles located near the rear of the fuselage.

The low-speed tests were conducted in the Langley V/STOL tunnel over an angle-of-attack range from -5° to 23° for all configurations. High angle-of-attack tests were conducted on selected configurations to extend the post-stall characteristics to angles of attack of approximately 38°. Static longitudinal and lateral stability characteristics were determined for the complete model and for the model with the tail surfaces removed. Tests of the fuselage and tail with the wing removed were also made to assess effects of the wing flow field on the tail contributions to both the longitudinal and lateral stability characteristics.

COEFFICIENTS AND SYMBOLS

The static-longitudinal and lateral-stability data are presented about the stability-axis system. The positive directions of forces, moments, and angles are shown in figure 1. The model moment reference point was located on the fuselage center line at the longitudinal location of the quarter-chord point of the mean aerodynamic chord of the theoretical (no wing root glove) wing planform.

The measurements of this investigation are presented in nondimensional coefficients, and the physical characteristics of the model and test conditions are presented in the International System of Units (SI). Details concerning the use of SI Units, together with physical constants and conversion factors, are presented in reference 6.

b	wing or tail surface span, cm
C_D	drag coefficient, Drag/qS
C_L	lift coefficient, Lift/qS
C_l	rolling-moment coefficient, Rolling moment/qSb
C_{l_β}	effective dihedral parameter, $\Delta C_l / \Delta\beta$, per deg ($\beta = \pm 5^{\circ}$)
C_m	pitching-moment coefficient, Pitching moment/$qS\bar{c}$
C_n	yawing-moment coefficient, Yawing moment/qSb
C_{n_β}	directional-stability parameter, $\Delta C_n / \Delta\beta$, per deg ($\beta = \pm 5^{\circ}$)
C_Y	side-force coefficient, Side force/qS
C_{Y_β}	side-force parameter, $\Delta C_Y / \Delta\beta$, per deg ($\beta = \pm 5^{\circ}$)
c	wing or tail surface chord, cm
$\bar{c}$	wing mean aerodynamic chord (theoretical planform), cm
$\bar{c}_H$	mean aerodynamic chord of horizontal tail, cm
$\bar{c}_V$	mean aerodynamic chord of vertical tail, cm
i_t	horizontal-tail incidence, positive when trailing edge is down, deg
q	free-stream dynamic pressure, N/m^2
S	wing area (based on theoretical planform, glove not included), m^2
t	airfoil thickness, cm
x	distance along chord (see tables), cm
x'	distance along flow-through nacelle center line, cm

y spanwise distance measured from fuselage center line, cm

z_l lower ordinate of airfoil section, cm

z_u upper ordinate of airfoil section, cm

α angle of attack of fuselage reference line, deg

β angle of sideslip, deg

ϵ effective downwash angle at horizontal tail (as obtained from tail-on and tail-off pitching-moment data), deg

$\Lambda_{c/4}$ quarter-chord sweep, deg

Λ_{LE} leading-edge sweep, deg

Designations:

F fuselage

H_1 high tail

H_2 mid tail

H_3 low tail

N_1 vertical-tail-mounted nacelle

$N_{1,2}$ vertical-tail-mounted nacelle plus outboard rear nacelles

V vertical tail

W wing

MODEL DESCRIPTION

The wing-body vertical-tail configuration used in the present investigation was scaled up from precision measurements of the configuration developed in the high-speed

tests of reference 3. A drawing of the basic high-tail model configuration is presented in figure 2(a), and details of the horizontal tails are shown in figures 2(b) and 2(c), and their vertical locations are shown in figure 2(d). Photographs of the model in the test section of the Langley V/STOL tunnel are presented in figure 3.

Wing

The complete wing, including the inboard glove, was machined from a single blank of aluminum to the planform shown in figure 2(a). The wing reference area, aspect ratio, and taper ratio were for the theoretical planform as defined by a linear extension of the leading edge and trailing edge to the plane of symmetry. The wing had 42° sweep of the quarter-chord line, an aspect ratio of 6.78, and a taper ratio of 0.36. Details of the wing-section coordinates for several spanwise locations are given in table I, and some basic geometric characteristics of the model are summarized in table II. Transition strips 0.23 cm wide of No. 80 carborundum grit were applied to the upper and lower surfaces of the wing, horizontal tail, and vertical tail 2.54 cm behind the leading edge, and on the fuselage 3.17 cm aft of the nose.

Fuselage

The basic cross-sectional shape of the fuselage was circular, with changes in the cross-sectional areas along the length to provide the desired area distribution when combined with the other configuration components. A fiber-glass-resin shell, 0.32 cm thick, formed the outer shape of the forward and middle sections of the fuselage and was attached to a metal strongback which held the wing and housed the six-component strain-gage balance. The rear section of the fuselage aft of the theoretical wing trailing edge at the plane of symmetry was constructed of cast aluminum. An electronic angle-of-attack sensor was mounted to the internal strongback to provide the geometric angle of attack of the model during the tests.

Tail Surfaces

The location and principal dimensions of the vertical tail and different horizontal tails investigated are given in figure 2. All the tail surfaces were constructed of aluminum and had symmetrical supercritical airfoil sections. The thickness of the horizontal tail was 0.09c at the root and varied linearly to 0.06c at the 0.40 semispan station and was 0.04c at the tip. The vertical tail was 0.12c thick. The coordinates of the tail surfaces are presented in tables III and IV. The horizontal tails were mounted on special brackets which were drilled to provide a range of stabilizer incidence angles from 5° to -15°.

The high tail was swept 45° at the leading edge, and the other two horizontal tails had 40° sweep. These different horizontal-tail planforms were constructed in response

to changes of tail geometry during the investigation of reference 3. The tip-to-tip span of the low horizontal tail was greater than that for the mid- and high-tail positions, and the longitudinal distance of the horizontal tail from the moment reference decreased as the tail location was lowered from the high-tail position. These significant differences in tail configurations do not, therefore, permit a detailed assessment of effects of tail height.

Nacelles

The basic model configuration with the high tail represented a three-engine arrangement with a central inlet just ahead of the base of the vertical tail and twin fuselage-mounted nacelles on the side and near the rear of the fuselage. Inasmuch as the model was sting mounted through the rear of the fuselage, no attempt was made to simulate airflow through a central nacelle. The central nacelle consisted of a swept wedge having a cross-sectional area equal to the nacelle area minus the stream-tube area. (See ref. 2 and figs. 2 and 3.) Twin fuselage-mounted nacelles were attached to the sides of the fuselage through stub pylons for some of the tests with the high horizontal tail. A constant (8.30 cm) internal diameter provided the opening for straight flow-through twin nacelles. (See table V for nacelle coordinates.)

TEST AND CORRECTIONS

The investigation was conducted in the Langley V/STOL tunnel at a dynamic pressure of 2394 N/m^2. The test Reynolds number at this dynamic pressure was 4.65×10^6 based on the wing mean aerodynamic chord of 0.306 m.

Longitudinal aerodynamic characteristics for all the model configurations were obtained from tests conducted through an angle-of-attack range from approximately -5° to 23°. An offset sting coupling was used in tests of some model configurations in order to obtain test data at high angles of attack to explore the deep-stall static aerodynamic characteristics. Tests made with the offset coupling extended over an angle-of-attack range from about 11° to 38°. Various stabilizer incidence angles were investigated for each model configuration to define the trimmed longitudinal characteristics over the test angle-of-attack range and to obtain effective downwash angles and stabilizer effectiveness. Tests were made with the horizontal tail removed to define the tail-off aerodynamic characteristics and wing-off tests were made to determine the effects of the wing flow field on the tail contributions to longitudinal and lateral aerodynamic characteristics.

Lateral-stability derivatives were obtained from tests conducted through the test angle-of-attack range with the model at sideslip angles of $\pm 5^{\circ}$. Lateral-stability tests were conducted with various components of the model removed, such as the horizontal tail, vertical tail, nacelles, and wing to determine the contribution of these components.

Jet-boundary corrections determined from reference 7 were added to the measured data; blockage corrections obtained from reference 8 were also applied to the data. The drag data were corrected for the balance chamber static pressure but have not been corrected for effects of flow through the nacelles. The small differences in drag at low angle of attack obtained with and without the nacelles in the investigation and that of reference 5 suggest that the drag increment associated with flow through the nacelles was negligible at low angles for the present low-speed investigation.

PRESENTATION OF RESULTS

The aerodynamic characteristics obtained for the various test conditions and model configurations are presented in the figures as follows:

DISCUSSION OF RESULTS

Longitudinal Characteristics

Effect of nacelles.- The longitudinal aerodynamic characteristics obtained over an angle-of-attack range up to about 24° are presented in figures 4 and 5 for the model with the high horizontal tail. Data obtained with the body-mounted twin nacelles in place are given in figure 4, and the characteristics without the nacelles are presented in figure 5. Comparison of the drag characteristics at low lift coefficients for the nacelles on and off (figs. 4 and 5) indicates very little difference in the drag coefficients obtained with and without the nacelles. These results indicate that the internal flow drag at low angles of attack of these flow-through nacelles was insignificant for these low-speed tests. The nacelles had very little effect on the overall trend of the aerodynamic characteristics, the largest effects being shown in higher drag and more negative pitching moments at high angles of attack with the nacelles on.

Lift characteristics.- The lift curves for both horizontal tail-on and tail-off configurations were fairly linear for angles of attack between $+5^{\circ}$ and -5°; above an angle of attack of $\approx 5^{\circ}$, the lift-curve slope began to decrease somewhat. (See figs. 4 and 5.) An appreciable reduction in lift-curve slope was indicated for angles of attack between 10° and 12°. This reduction in lift-curve slope is indicative of appreciable changes in the flow over the wing at moderately high angles of attack. The increasing instability shown in the pitching moments for the tail-off configuration (fig. 5, for example) as the angle of attack increased from the lowest test angle to moderate angles suggests that flow changes, probably leading-edge vortex formation, started early and increased as the lift increased.

Lift characteristics obtained over an extended angle-of-attack range (figs. 8 and 9) indicated that the maximum lift coefficient of the wing-body configuration was about 1.46. Addition of the high tail (fig. 8) did not provide appreciable increases in maximum lift, whereas addition of the low tail (fig. 9) increased the maximum lift coefficient to at least 1.80. The added lift of the low tail may be attributed primarily to an improved flow field at the tail and to the fact that the low tail had somewhat more effective area than the higher tail.

Extended angle-of-attack range.- Tests were conducted for the high tail and the low tail over an extended angle-of-attack range from about 11° to 38° in order to explore the deep-stall region. There was an overlap region of angles of attack between 11° and 24° where data were obtained both in the low and high angle-of-attack range. Test results for the tail-off and high-tail configurations showed excellent agreement (see fig. 8) between the two sets of overlapping data. Results obtained for the low-tail configuration showed slightly higher lift at a given angle of attack in the overlap region for the high angle-of-attack range. The agreement in tail-on pitching moments for the low tail was not partic-

larly good. Pitching moments were more negative for the high angle-of-attack range data than for the low angle-of-attack range data when the tail contribution was negative and more positive for the high angle-of-attack range where the tail contribution was positive. (See fig. 9.) Also, the pitching moments from the two sets of tail-on data were in agreement for angles of attack near zero tail load where the tail-on data crossed the tail-off data.

The apparent augmentation of the tail load evident in the data for the high angle-of-attack range had a significant effect on the tail effectiveness parameter $\partial C_m/\partial i_t$ for the low tail which was about 25 percent greater for the data for the high angle-of-attack range (fig. 15) than for the data for the low angle-of-attack range. Comparison of the values of $\partial C_m/\partial i_t$ for the low angle-of-attack range obtained with the low tail and the wing removed (fig. 16) shows good agreement with the data for the high angle-of-attack range for the complete model (fig. 15) for angles of attack between 12° and 15°.

The differences in results obtained with the low tail may be associated with differences in flow over the rear part of the model and the support sting when the low tail was lifting. These differences in pitching moments affect the stabilizer setting for trim but do not alter any overall conclusions that could be drawn from the data in regard to the stability characteristics and the capability of the horizontal tail to function as a longitudinal control.

Effects of tail configuration.- The pitching-moment characteristics of the model with the high tail (fig. 5) showed an abrupt loss of stability near an angle of attack of 10° which persisted to an angle of attack of about 25° where the pitching moments became stable. This large loss of stability can be attributed primarily to an increase in the downwash gradient $\partial\epsilon/\partial\alpha$ at the tail (see fig. 15) which caused the high tail to be destabilizing ($\partial\epsilon/\partial\alpha > 1.0$) for angles of attack between 16° and 26°.

Effects of tail configuration on pitching moments obtained with 0° stabilizer setting are presented in figure 13. The pitching-moment comparison shows that both the mid tail and low tail have a loss of stability at slightly lower angles of attack than for the high tail and tend to recover stability at lower angles of attack than the high tail. The low-tail configuration showed a range of instability for angles of attack from about 6° to 16°; whereas the high tail was unstable for angles of attack between 10° and 26°.

The instability shown for the high and mid tails can be attributed primarily to the loss in tail contribution associated with the downwash gradient exceeding a value of unity. Downwash gradients for the low tail, however, never exceeded 0.8. Therefore, the tail was providing a stabilizing contribution throughout the entire angle-of-attack range. The low-tail configuration did not provide sufficient contribution to stability to overcome the large increasing instability of the tail-off configuration for angles of attack between 6° and 16°. (See fig. 8.)

The longitudinal instability encountered on the model can be attributed basically to flow changes on the wing, which caused the wing-body configuration to become increasingly unstable at moderate angles of attack, and which also caused large destabilizing changes in the flow field of both the high- and mid-tail heights. Inasmuch as the basic stability problem was flow over the wing, flow-control devices or other appropriate modifications to the wing would be required to achieve more satisfactory static longitudinal stability characteristics of this configuration.

Lateral-Stability Derivatives

The static lateral-stability derivatives of the model over an extended angle-of-attack range are presented in figure 17 for the high tail and figure 18 for the low tail. Results obtained with the horizontal tail removed and with the horizontal and vertical tail removed are presented to allow assessment of the effects of these components. The flow changes over the wing (horizontal tail off) indicated in the longitudinal data around an angle of attack of 10° are also indicated in the lateral derivatives.

Effective dihedral parameter.- The effective dihedral parameter C_{l_β} showed positive effective dihedral for the basic wing body in that negative values of C_{l_β} occurred at positive lifting conditions. There is an abrupt decrease of C_{l_β} shown as the angle of attack increased beyond 10° (fig. 17). However, no reversal in the sign of C_{l_β} was indicated at moderate or high lift. Addition of the vertical tail (fig. 17) increased the effective dihedral $\left(-C_{l_\beta}\right)$ inasmuch as the center of pressure of the yawed vertical tail was above the moment reference axis. Addition of the high horizontal tail to the vertical tail (fig. 17) provided an end-plate effect on the lateral derivatives as indicated by the increased values of all the derivatives that accompanied the addition of the high tail. Addition of the low tail (fig. 18) had little effect on the lateral derivatives, possibly because the fuselage provided most of the attainable end-plate effect that could be realized for the root portion of the vertical tail. Lateral stability characteristics with the mid-horizontal tail were generally about the same as for the low tail except that at low angles of attack the mid-tail configuration had less directional stability than the low tail. (See fig. 20.)

Directional stability.- The wing-body configuration showed static directional instability over the angle-of-attack range of the investigation (fig. 17); the level of instability at an angle of attack of 35° was more than twice the instability at low angles of attack (up to 15°). Addition of the tail surfaces provided positive directional stability at low and moderate angles of attack; however, the large loss in directional stability that occurred as the angle of attack increased beyond 15° caused the complete model to become directionally unstable at angles above 30° for the high-tail configuration and above 24° for the low-tail configuration. The directional instability at high angles of attack occurred

because of destabilizing sidewash flow over the vertical tail as evidenced by the continuing decrease of tail contribution to C_{n_β} and the greater instability with the tail on than with the vertical tail off at the highest angles of attack. The occurrence of positive values of C_{Y_β} at the highest angles of attack also suggest that significant sidewash effects were present. It should be noted, however, that the high angles of attack studied represent possible deep-stall conditions and are much beyond the normal expected operational angle-of-attack range for a transport airplane.

Effects of twin nacelles.- Lateral-stability derivatives obtained both with and without the twin fuselage-mounted nacelles are presented in figure 19. These test results show that the effects of adding the twin nacelles were generally small throughout the test angle-of-attack range. The twin nacelles provided a small positive increment to directional stability, but the simulated central nacelle added to the vertical tail reduced the directional stability slightly.

SUMMARY OF RESULTS

The results of a low-speed wind-tunnel investigation of a transport airplane configuration having a 42° swept wing and low, mid, and high horizontal-tail positions may be summarized as follows:

1. Both the static longitudinal and lateral aerodynamic characteristics of the model were dominated by unfavorable flow development over the swept wing from moderate to high angles of attack.

2. Effects of the unfavorable flow changes on the longitudinal stability were evidenced in the wing-body pitching moments which became more unstable as the angle of attack increased up to about 15°. With either a high, mid, or low horizontal-tail position, the model became longitudinally unstable for angles of attack above about 10°; the degree of instability was least for the low tail and increased as the tail height increased.

3. The high longitudinal instability of the model with both the mid- and high-tail positions was found to be a result of highly destabilizing increases in downwash gradient at the tail. The stabilizer effectiveness of the model with each of the tail configurations remained relatively high throughout the angle-of-attack range of the investigation.

4. Static lateral-stability derivatives of the model indicated positive effective dihedral throughout the angle-of-attack range of the investigation. Positive static-directional stability was indicated at low and moderate angles of attack with the vertical tail on, for all horizontal-tail configurations tested. However, the tail contribution generally decreased as the angle of attack increased, and directional instability occurred for angles above about 24° with the low horizontal tail. Addition of the high horizontal tail provided

a substantial end-plate effect which extended the angle at which directional instability occurred to approximately 30°.

5. The directional instability shown for the complete model was caused by destabilizing sidewash. At high angles of attack, the complete model was more unstable than the model with the tail surfaces removed. It should be noted, however, that the high angles of attack studied represent possible deep-stall conditions and are much beyond the normal expected operational angle-of-attack range for a transport airplane.

Langley Research Center,
National Aeronautics and Space Administration,
Hampton, Va., November 7, 1974.

REFERENCES

1. Whitcomb, Richard T.; and Clark, Larry R.: An Airfoil Shape for Efficient Flight at Supercritical Mach Numbers. NASA TM X-1109, 1965.

2. Harris, Charles D.: Wind-Tunnel Investigation of Effects of Trailing-Edge Geometry on a NASA Supercritical Airfoil Section. NASA TM X-2336, 1971.

3. Langhans, Richard A.; and Flechner, Stuart G.: Wind-Tunnel Investigation at Mach Numbers From 0.25 to 1.01 of a Transport Configuration Designed To Cruise at Near-Sonic Speeds. NASA TM X-2622, 1972.

4. Fournier, Paul G.; and Goodson, Kenneth W.: Low-Speed Aerodynamic Characteristics of a 42° Swept High-Wing Model Having a Double-Slotted Flap System and a Supercritical Airfoil. NASA TM X-3036, 1974.

5. Fournier, Paul G.; and Sleeman, William C., Jr.: Low-Speed Aerodynamic Characteristics of a Model Having a 42° Swept Low Wing With a Supercritical Airfoil, Double-Slotted Flaps, and a T-Tail. NASA TM X-2582, 1972.

6. Mechtly, E. A.: The International System of Units – Physical Constants and Conversion Factors (Second Revision). NASA SP-7012, 1973.

7. Gillis, Clarence L.; Polhamas, Edward C.; and Gray, Joseph L., Jr.: Charts for Determining Jet-Boundary Corrections for Complete Models in 7- by 10-Foot Closed Rectangular Wind Tunnels. NACA WR L-123, 1945. (Formerly NACA ARR L5G31.)

8. Herriot, John G.: Blockage Corrections for Three-Dimensional-Flow Closed-Throat Wind Tunnels, With Consideration of the Effect of Compressibility. NACA Rep. 995, 1950. (Supersedes NACA RM A7B28.)

TABLE I.- WING AIRFOIL COORDINATES

x/c	z_u/c	z_l/c	z_u/c	z_l/c	z_u/c	z_l/c	z_u/c	z_l/c	z_u/c	z_l/c
	$\frac{y}{b/2} = 0.083$; $c = 103.175$ cm		$\frac{y}{b/2} = 0.140$; $c = 77.638$ cm		$\frac{y}{b/2} = 0.186$; $c = 60.086$ cm		$\frac{y}{b/2} = 0.279$; $c = 39.634$ cm		$\frac{y}{b/2} = 0.372$; $c = 32.182$ cm	
0	-0.0495	-0.0495	-0.0804	-0.0804	-0.1181	-0.1181	-0.2095	-0.2095	-0.2760	-0.2760
.0025	-.0421	-.0550	-.0732	-.0871	-.1108	-.1255	-.2002	-.2167	-.2692	-.2841
.0050	-.0399	-.0570	-.0707	-.0894	-.1084	-.1278	-.1969	-.2201	-.2663	-.2877
.0100	-.0371	-.0598	-.0677	-.0925	-.1048	-.1314	-.1926	-.2241	-.2618	-.2916
.0200	-.0337	-.0635	-.0638	-.0967	-.1003	-.1364	-.1868	-.2297	-.2565	-.2966
.0300	-.0313	-.0667	-.0612	-.1002	-.0979	-.1403	-.1831	-.2336	-.2529	-.2999
.0400	-.0295	-.0692	-.0590	-.1030	-.0945	-.1434	-.1800	-.2369	-.2501	-.3029
.0700	-.0251	-.0753	-.0543	-.1097	-.0894	-.1503	-.1746	-.2435	-.2447	-.3079
.1000	-.0222	-.0805	-.0511	-.1148	-.0862	-.1557	-.1712	-.2483	-.2410	-.3114
.1500	-.0192	-.0870	-.0474	-.1215	-.0829	-.1624	-.1677	-.2537	-.2365	-.3150
.2000	-.0175	-.0924	-.0455	-.1271	-.0809	-.1678	-.1652	-.2577	-.2330	-.3171
.3000	-.0177	-.1010	-.0454	-.1354	-.0796	-.1754	-.1635	-.2612	-.2293	-.3186
.4000	-.0206	-.1068	-.0482	-.1402	-.0823	-.1790	-.1648	-.2604	-.2289	-.3172
.5000	-.0256	-.1093	-.0539	-.1418	-.0875	-.1785	-.1683	-.2559	-.2300	-.3127
.6000	-.0338	-.1088	-.0617	-.1399	-.0953	-.1741	-.1737	-.2471	-.2321	-.3037
.7000	-.0453	-.1045	-.0724	-.1327	-.1049	-.1647	-.1803	-.2353	-.2357	-.2889
.7500	-.0516	-.1004	-.0783	-.1272	-.1103	-.1582	-.1842	-.2286	-.2384	-.2803
.8000	-.0580	-.0960	-.0844	-.1218	-.1158	-.1519	-.1885	-.2218	-.2414	-.2721
.8500	-.0648	-.0910	-.0908	-.1166	-.1215	-.1466	-.1928	-.2163	-.2454	-.2658
.9000	-.0721	-.0875	-.0974	-.1128	-.1274	-.1428	-.1975	-.2133	-.2495	-.2632
.9500	-.0801	-.0874	-.1045	-.1124	-.1335	-.1422	-.2033	-.2137	-.2553	-.2659
.9700	-.0835	-.0889	-.1075	-.1136	-.1360	-.1431	-.2057	-.2150	-.2580	-.2682
.9800	-.0854	-.0901	-.1091	-.1145	-.1373	-.1438	-.2070	-.2160	-.2595	-.2696
.9900	-.0871	-.0916	-.1106	-.1157	-.1386	-.1448	-.2084	-.2171	-.2612	-.2712
1.0000	-.0891	-.0933	-.1122	-.1172	-.1398	-.1460	-.2099	-.2185	-.2630	-.2729

TABLE I.- WING AIRFOIL COORDINATES – Concluded

x/c	z_u/c	z_l/c	z_u/c	z_l/c	z_u/c	z_l/c	z_u/c	z_l/c	z_u/c	z_l/c
	$\frac{y}{b/2} = 0.400$; c = 31.316 cm		$\frac{y}{b/2} = 0.512$; c = 28.491 cm		$\frac{y}{b/2} = 0.933$; c = 17.854 cm		$\frac{y}{b/2} = 1.000$; c = 16.147 cm		$\frac{y}{b/2} = 1.035$; c = 15.258 cm	
0	-0.2880	-0.2880	-0.3310	-0.3310	-0.6150	-0.6150	-0.6954	-0.6954	-0.7444	-0.7444
.0025	-.2801	-.2968	-.3233	-.3394	-.6085	-.6217	-.6893	-.7015	-.7385	-.7503
.0050	-.2774	-.2996	-.3206	-.3421	-.6064	-.6236	-.6872	-.7033	-.7365	-.7519
.0100	-.2734	-.3036	-.3167	-.3460	-.6028	-.6263	-.6837	-.7057	-.7331	-.7539
.0200	-.2682	-.3084	-.3116	-.3505	-.5982	-.6296	-.6795	-.7086	-.7288	-.7568
.0300	-.2649	-.3115	-.3083	-.3537	-.5951	-.6320	-.6763	-.7108	-.7257	-.7588
.0400	-.2625	-.3140	-.3059	-.3559	-.5929	-.6335	-.6742	-.7121	-.7237	-.7598
.0700	-.2571	-.3189	-.3005	-.3606	-.5872	-.6361	-.6683	-.7142	-.7178	-.7616
.1000	-.2536	-.3221	-.2971	-.3634	-.5826	-.6366	-.6636	-.7139	-.7128	-.7610
.1500	-.2492	-.3256	-.2922	-.3664	-.5764	-.6361	-.6569	-.7123	-.7058	-.7589
.2000	-.2463	-.3225	-.2889	-.3680	-.5706	-.6344	-.6503	-.7100	-.6990	-.7558
.3000	-.2426	-.3287	-.2844	-.3683	-.5608	-.6294	-.6389	-.7033	-.6867	-.7484
.4000	-.2410	-.3268	-.2819	-.3657	-.5519	-.6227	-.6283	-.6954	-.6750	-.7397
.5000	-.2410	-.3219	-.2808	-.3603	-.5440	-.6136	-.6185	-.6853	-.6639	-.7289
.6000	-.2421	-.3130	-.2809	-.3508	-.5373	-.6004	-.6100	-.6710	-.6540	-.7141
.7000	-.2451	-.2979	-.2828	-.3350	-.5320	-.5809	-.6023	-.6506	-.6456	-.6930
.7500	-.2473	-.2884	-.2844	-.3254	-.5299	-.5702	-.5994	-.6392	-.6417	-.6817
.8000	-.2503	-.2798	-.2870	-.3166	-.5287	-.5603	-.5973	-.6291	-.6388	-.6714
.8500	-.2540	-.2735	-.2901	-.3103	-.5289	-.5524	-.5965	-.6212	-.6377	-.6627
.9000	-.2585	-.2717	-.2948	-.3079	-.5306	-.5479	-.5973	-.6158	-.6380	-.6572
.9500	-.2644	-.2749	-.3011	-.3112	-.5356	-.5483	-.6021	-.6156	-.6425	-.6564
.9700	-.2674	-.2775	-.3045	-.3145	-.5395	-.5507	-.6060	-.6177	-.6465	-.6584
.9800	-.2690	-.2790	-.3065	-.3164	-.5419	-.5524	-.6084	-.6193	-.6491	-.6599
.9900	-.2708	-.2808	-.3088	-.3188	-.5443	-.5546	-.6111	-.6212	-.6516	-.6620
1.0000	-.2727	-.2828	-.3115	-.3214	-.5469	-.5570	-.6137	-.6238	-.6541	-.6643

TABLE II.- GEOMETRIC CHARACTERISTICS

Wing (theoretical):	
Area, m^2	0.530
Mean aerodynamic chord, cm	30.638
Span, cm	184.068
Aspect ratio	6.394
Taper ratio	0.390
$\Lambda_{c/4}$, deg	42.27
Horizontal tails:	
Area, m^2	0.124
Mean aerodynamic chord, cm	21.570
Span, cm	60.985
Aspect ratio	3.000
Taper ratio	0.401
Λ_{LE}, deg:	
H_1 (high tail)	45
H_2 (mid tail)	40
H_3 (low tail)	40
Vertical tail:	
Area, m^2	0.113
Mean aerodynamic chord, cm	37.247
Span, cm	30.599
Aspect ratio	0.831
Taper ratio	0.687
Λ_{LE}, deg	50

TABLE III.- HORIZONTAL-TAIL AIRFOIL COORDINATES

[Symmetrical airfoil sections]

x/c	1/2(t/c)	1/2(t/c)	1/2(t/c)
	$\frac{y}{b/2}$ = 0; c = 29.017 cm	$\frac{y}{b/2}$ = 0.4000; c = 22.068 cm	$\frac{y}{b/2}$ = 1.0000; c = 11.640 cm
0	0	0	0
.0100	.0162	.0093	.0094
.0200	.0219	.0129	.0129
.0300	.0258	.0151	.0151
.0500	.0312	.0185	.0185
.1000	.0389	.0236	.0236
.1500	.0427	.0265	.0266
.2000	.0445	.0283	.0284
.2500	.0450	.0294	.0292
.3000	.0446	.0298	.0299
.3500	.0435	.0300	.0299
.4000	.0418	.0298	.0299
.4500	.0397	.0294	.0292
.5000	.0373	.0286	.0284
.5500	.0345	.0274	.0272
.6000	.0314	.0259	.0260
.6500	.0281	.0242	.0242
.7000	.0246	.0221	.0220
.7500	.0209	.0197	.0196
.8000	.0170	.0169	.0170
.8500	.0130	.0139	.0140
.9000	.0088	.0106	.0107
.9500	.0044	.0069	.0070
1.0000	0	.0030	.0030

TABLE IV.- VERTICAL-TAIL AIRFOIL COORDINATES

[c = 43.6550 cm at root and 30.0000 cm at tip; symmetrical airfoil sections]

x/c	1/2(t/c)
0	0
.0100	.0187
.0200	.0254
.0300	.0301
.0400	.0339
.0500	.0370
.0600	.0396
.0700	.0419
.0800	.0439
.0900	.0456
.1000	.0472
.1500	.0530
.2000	.0566
.2500	.0587
.3000	.0597
.3500	.0600
.4000	.0596
.4500	.0586
.5000	.0570
.5500	.0547
.6000	.0516
.6500	.0483
.7000	.0441
.7500	.0394
.8000	.0339
.8500	.0279
.9000	.0212
.9500	.0139
1.0000	.0059

TABLE V.- COORDINATES OF FLOW-THROUGH NACELLES

[Inside diameter, 8.30 cm]

x', cm	Radius, cm		
	Inboard side	Outboard side	Top and bottom
-2.354		4.237	
-1.069		4.493	4.280
0	4.280	4.666	4.536
2.139	4.793	4.922	4.879
4.280	5.093	5.136	5.093
6.421	5.265	5.306	5.265
8.560	5.349	5.392	5.349
10.698	5.392	5.436	5.392
12.840	5.436	5.436	5.436
14.981	5.392	5.392	5.392
17.120	5.349	5.349	5.349
19.261	5.179	5.179	5.179
21.400	5.006	5.006	5.006
23.541	4.793	4.793	4.793
25.679	4.536	4.536	4.536
27.821	4.323	4.323	4.323
29.616	4.150	4.150	4.150

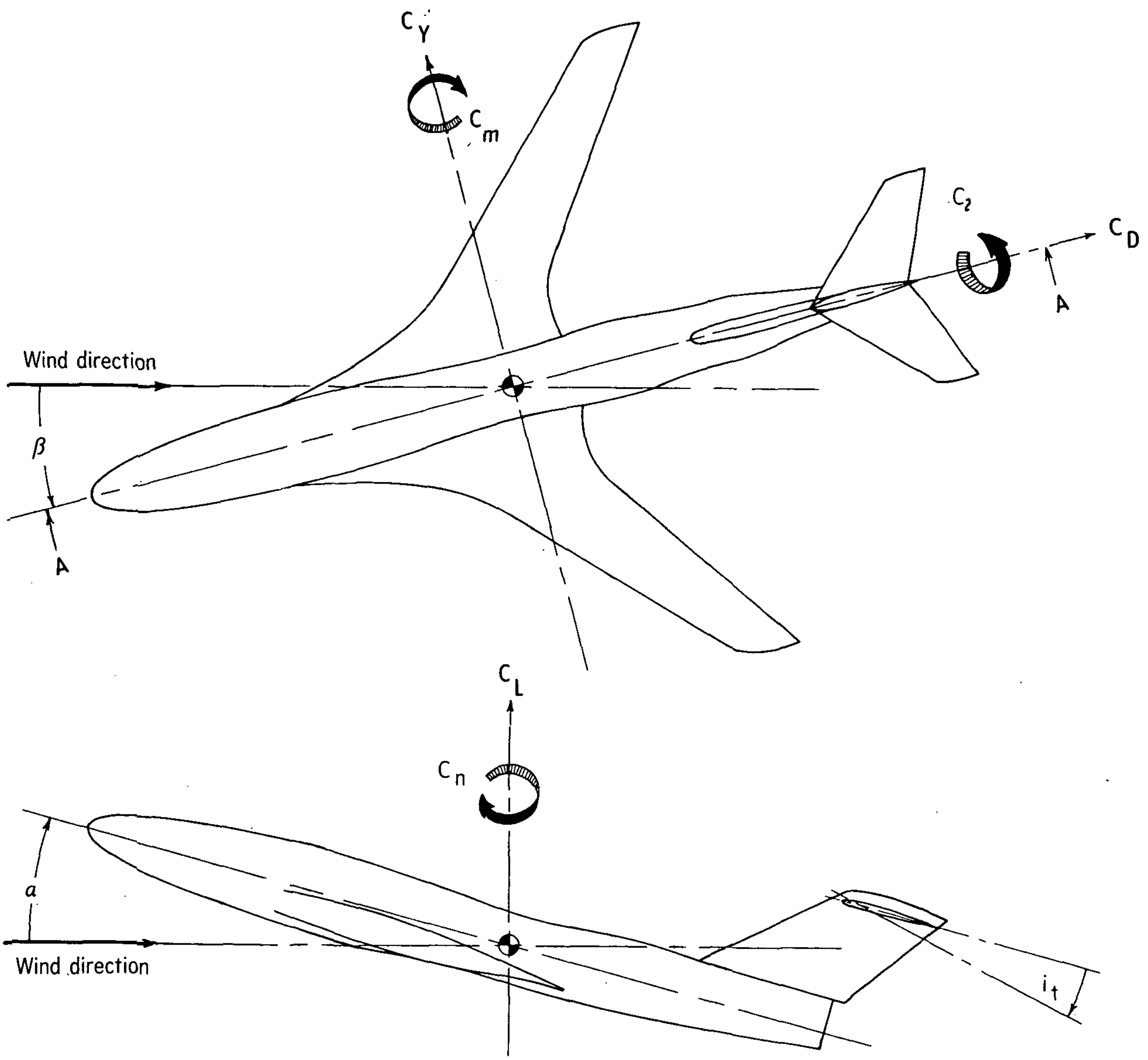

View A-A

Figure 1.- System of axes. Positive directions of forces, moments, and angles are indicated by arrow.

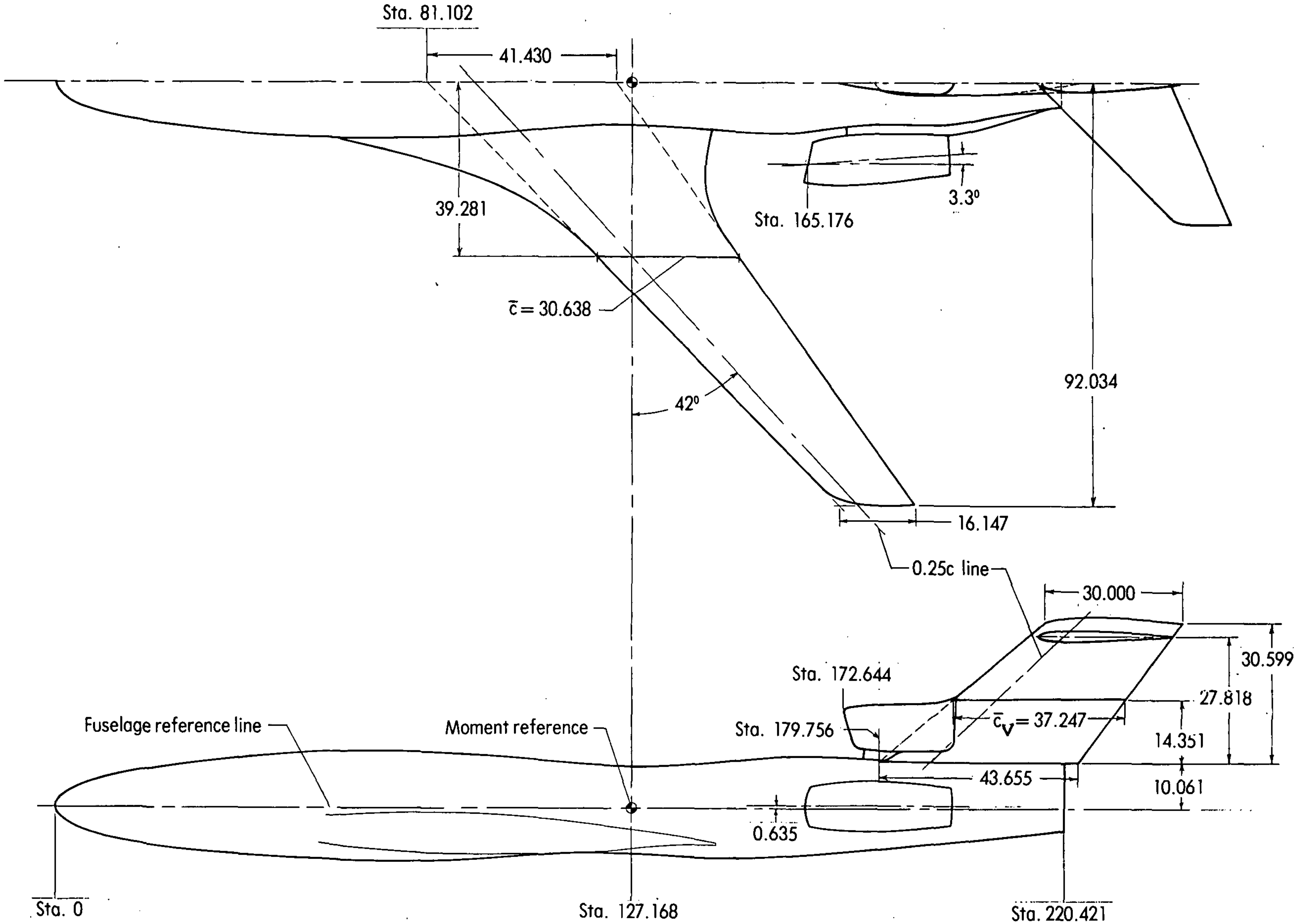

(a) Complete model.

Figure 2.- Details of model. Dimensions are in centimeters.

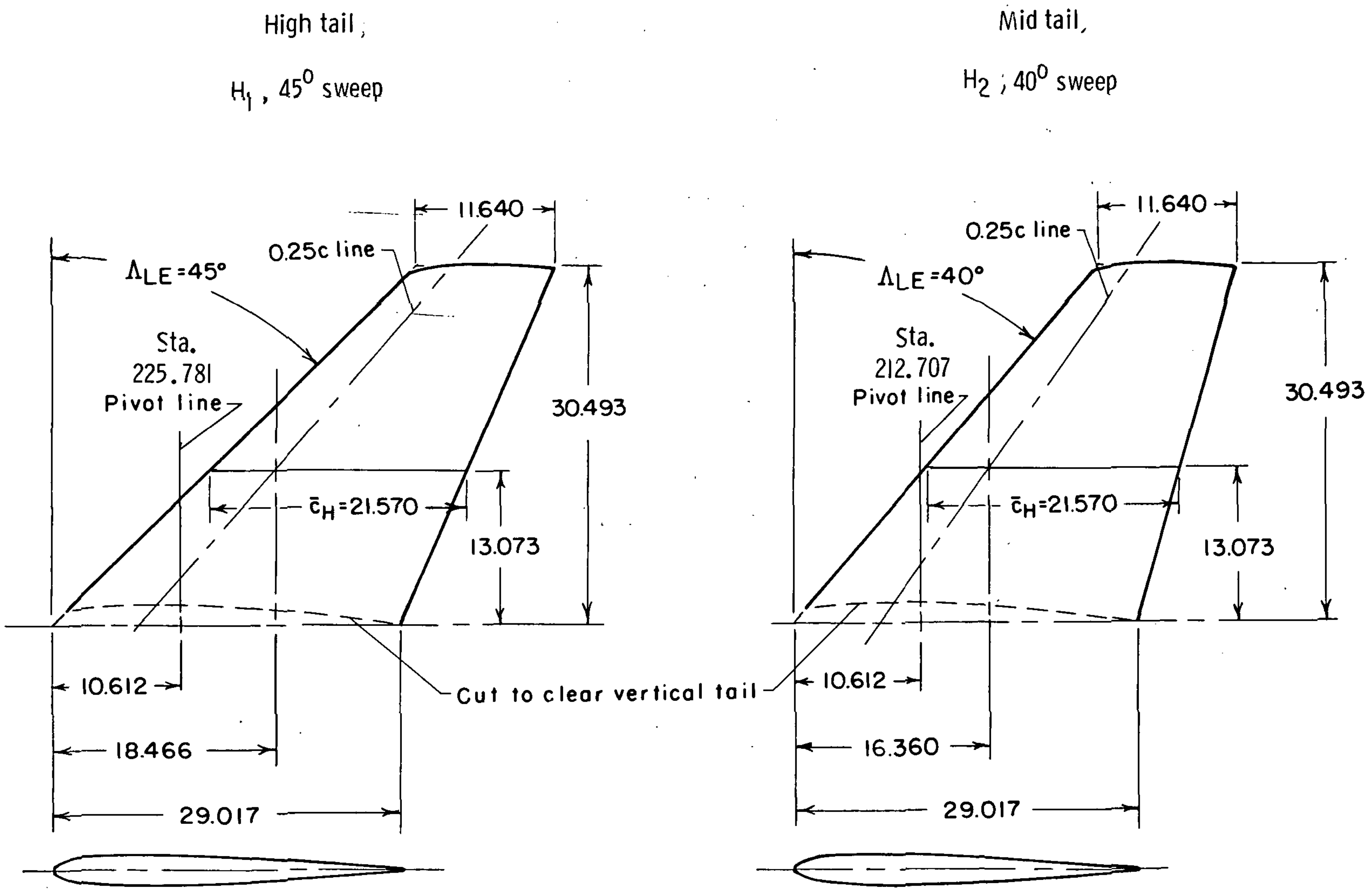

(b) Horizontal tails.

Figure 2.- Continued.

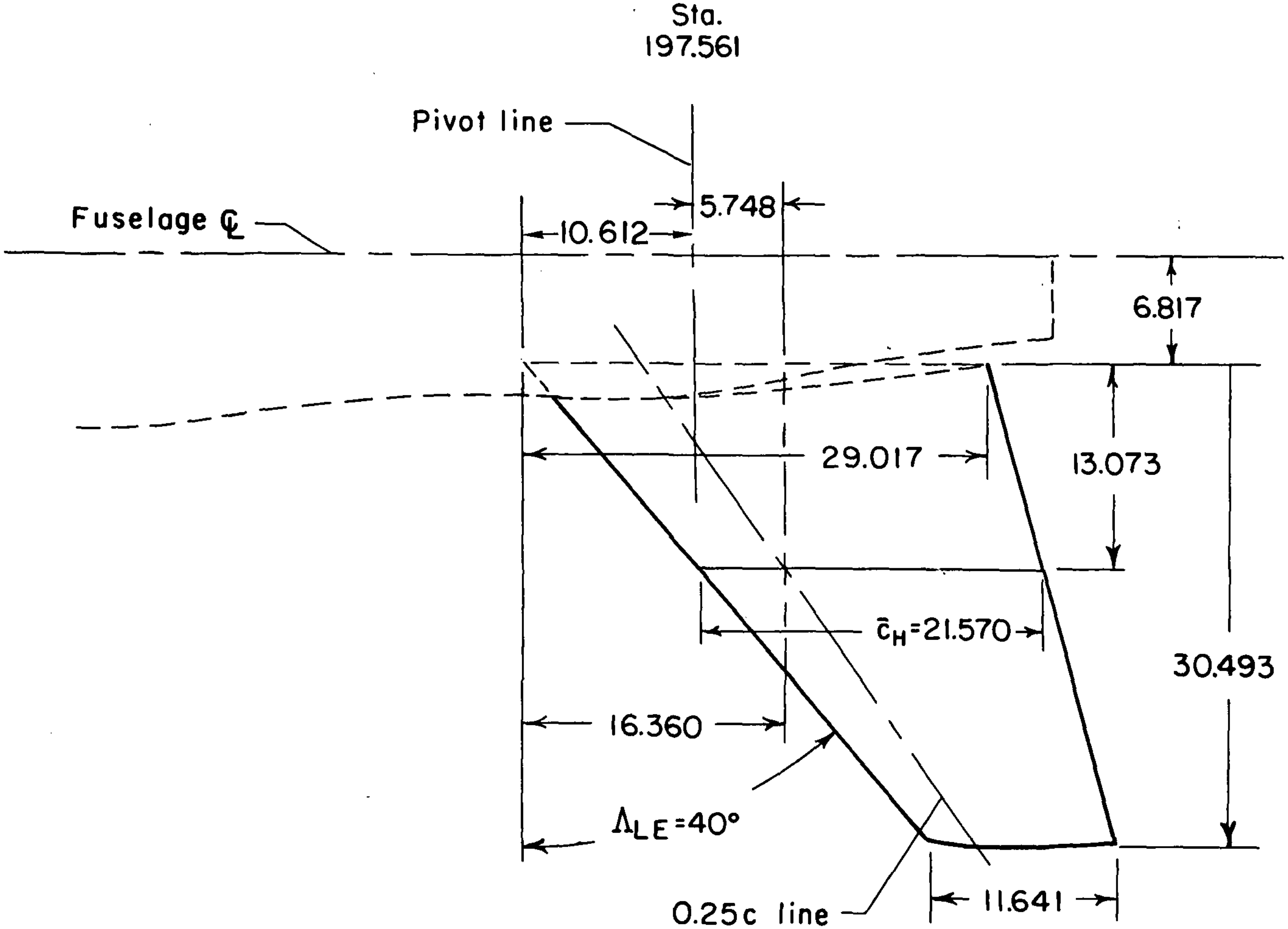

(c) H_3, 40^o sweep low tail.

Figure 2.- Continued.

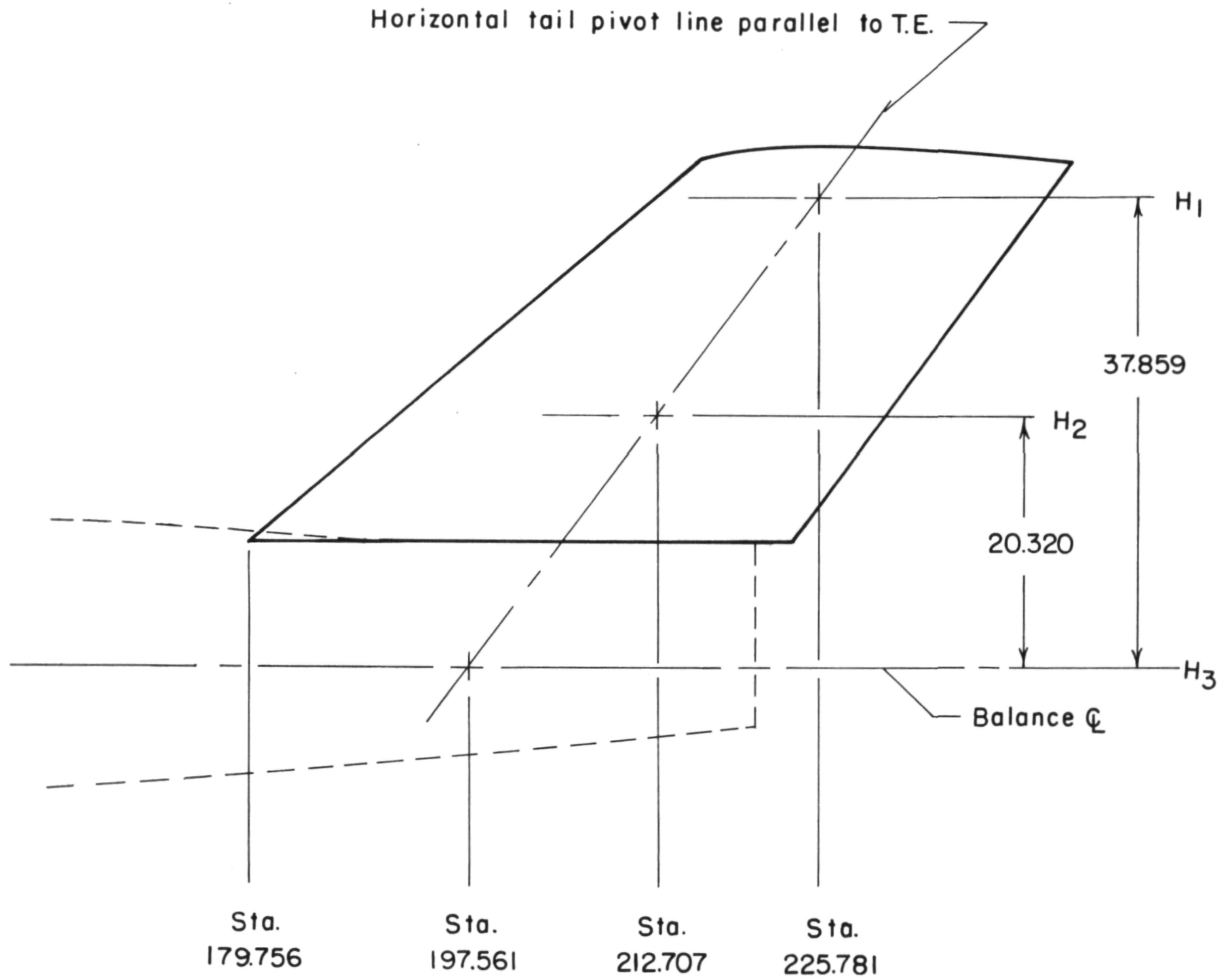

(d) Horizontal-tail height and pivot location.

Figure 2.- Concluded.

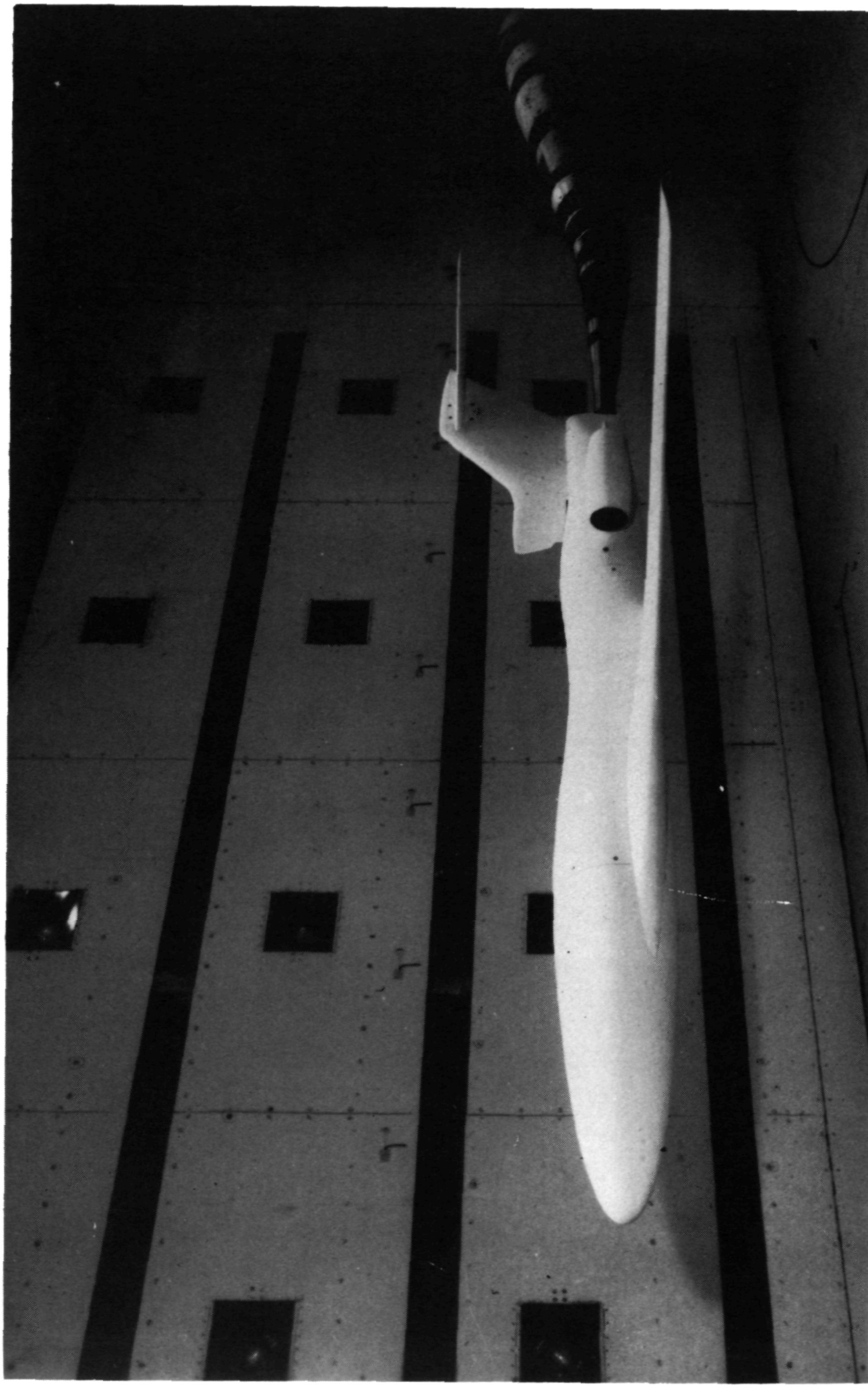

L-72-4272

(a) Three-quarter front view.

Figure 3.- Photographs of model in Langley V/STOL tunnel. Complete configuration.

L-72-4275

(b) Side view.

Figure 3.- Continued.

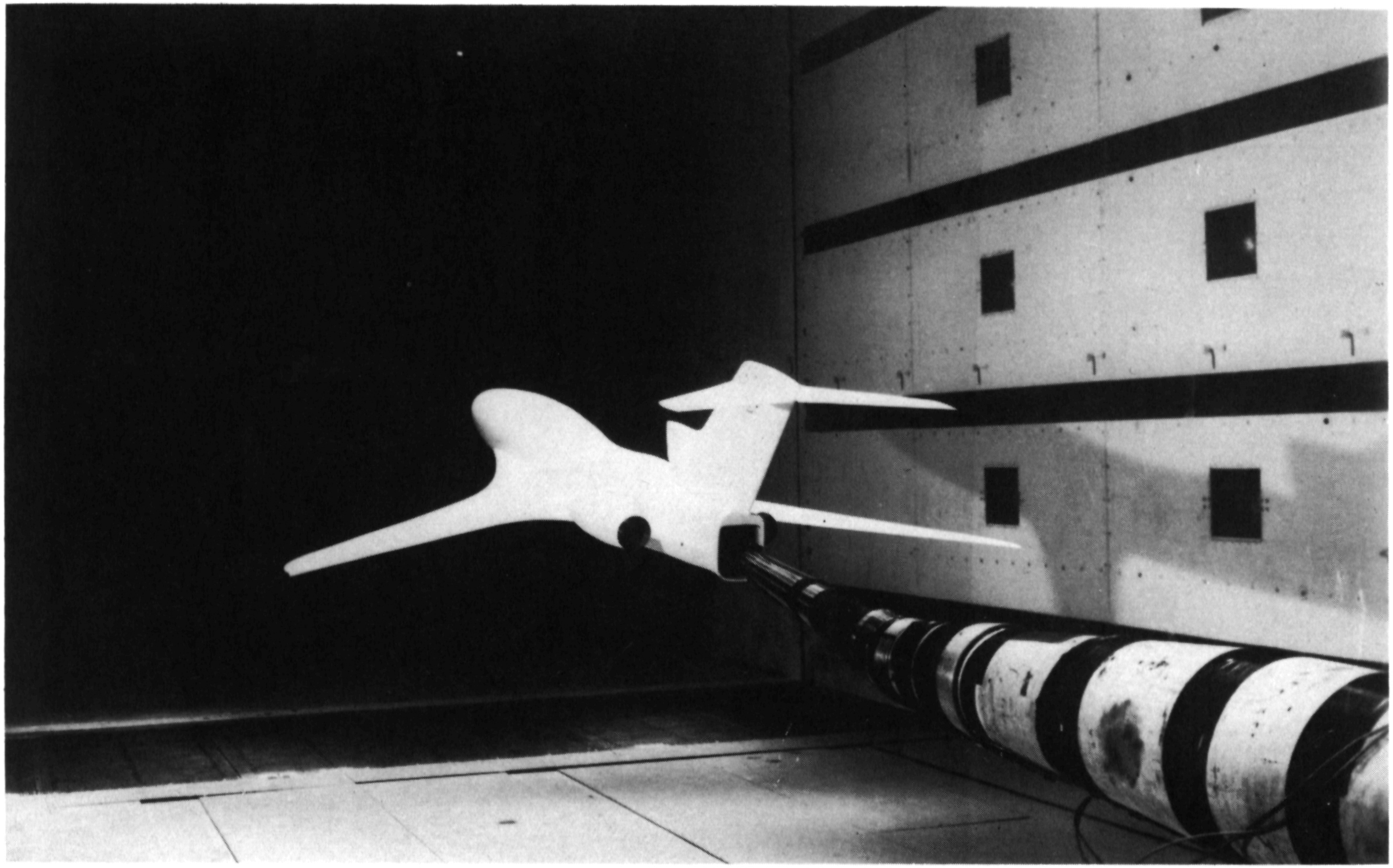

L-72-4274

(c) Three-quarter rear view.

Figure 3.- Concluded.

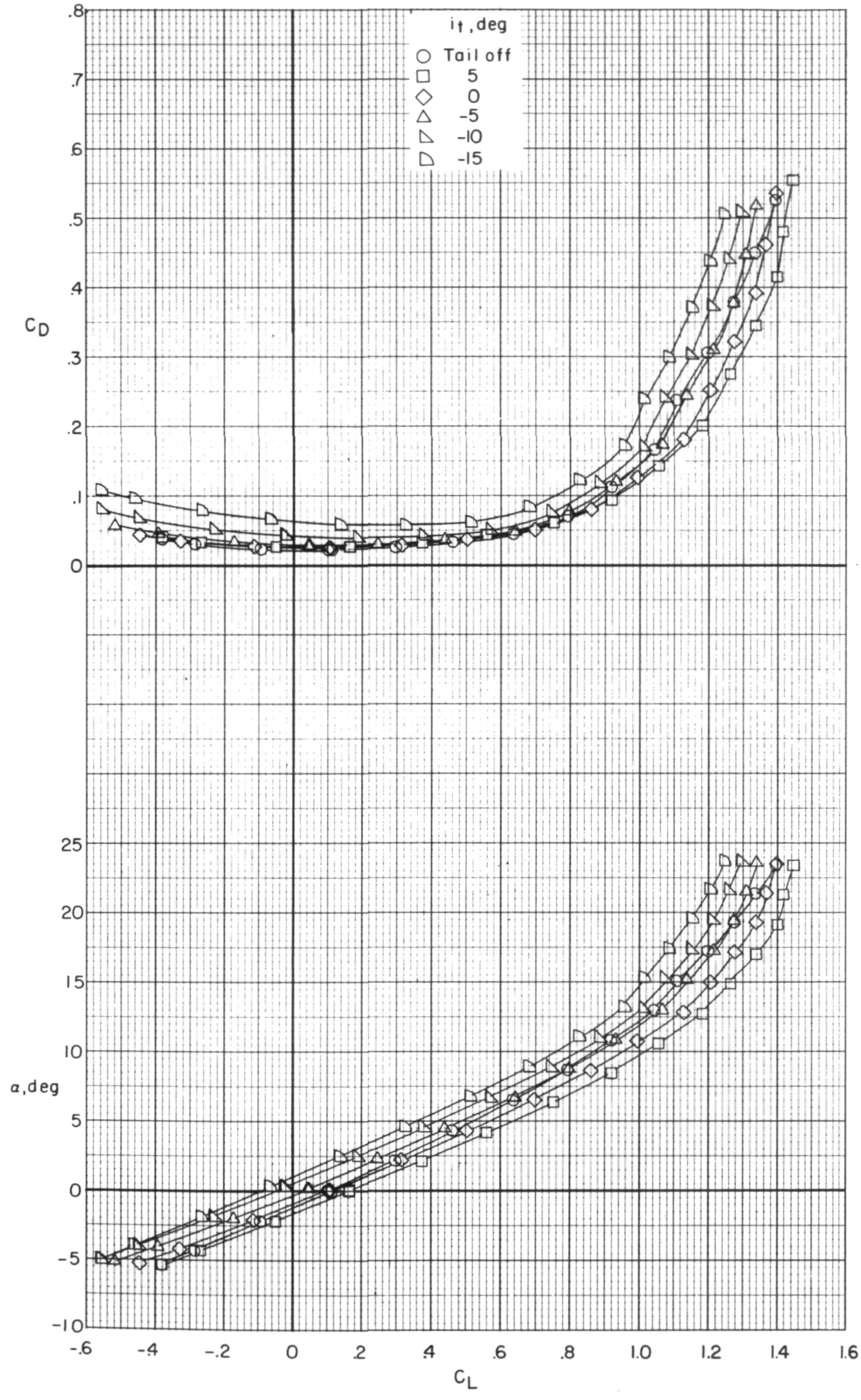

Figure 4.- Effect of horizontal-tail deflection on longitudinal aerodynamic characteristics. Complete model with high tail; $WFVH_1N_{1,2}$.

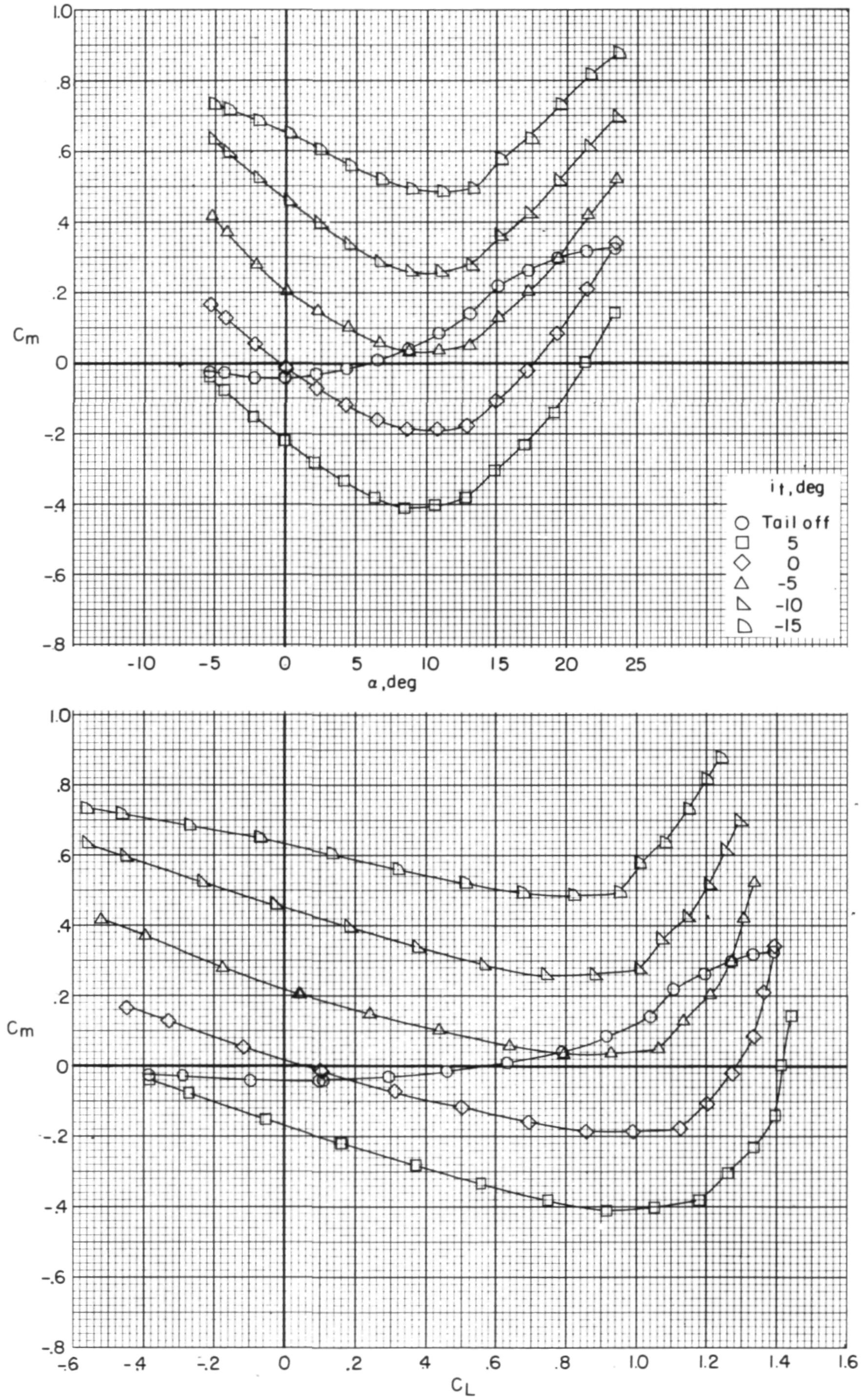

Figure 4.- Concluded.

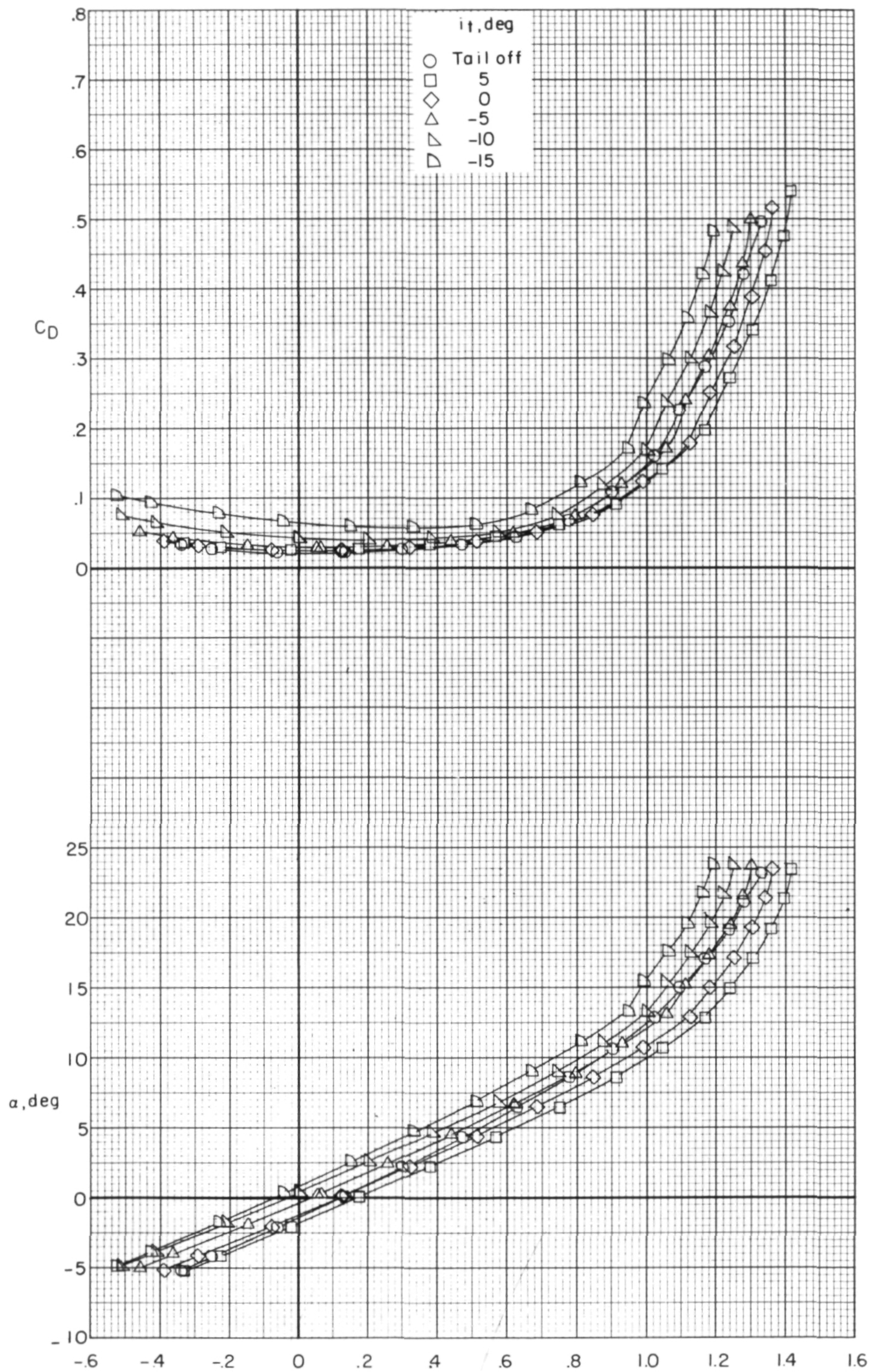

Figure 5.- Effect of horizontal-tail deflection on longitudinal aerodynamic characteristics. Nacelles removed, high tail; $WFVH_1$.

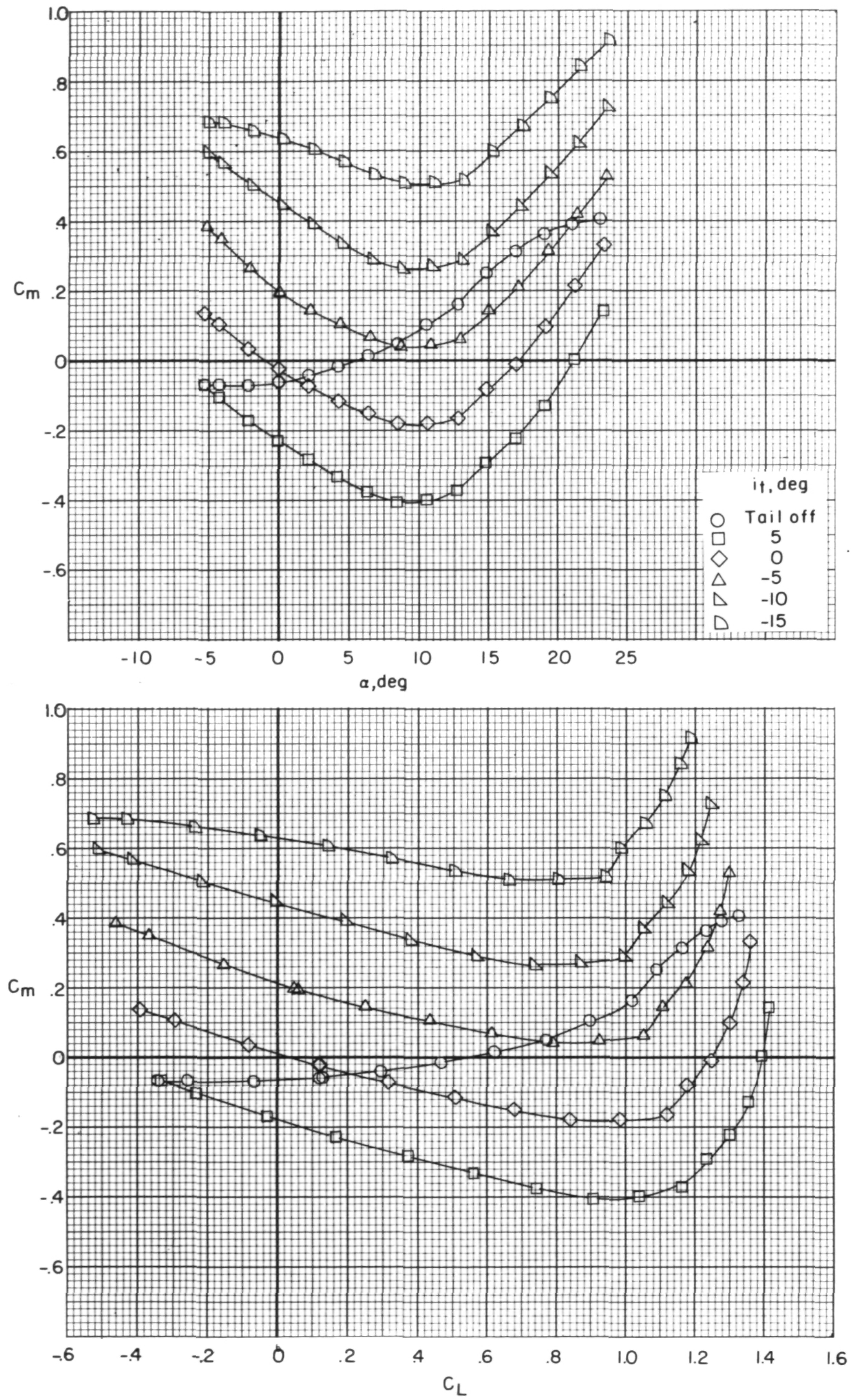

Figure 5.- Concluded.

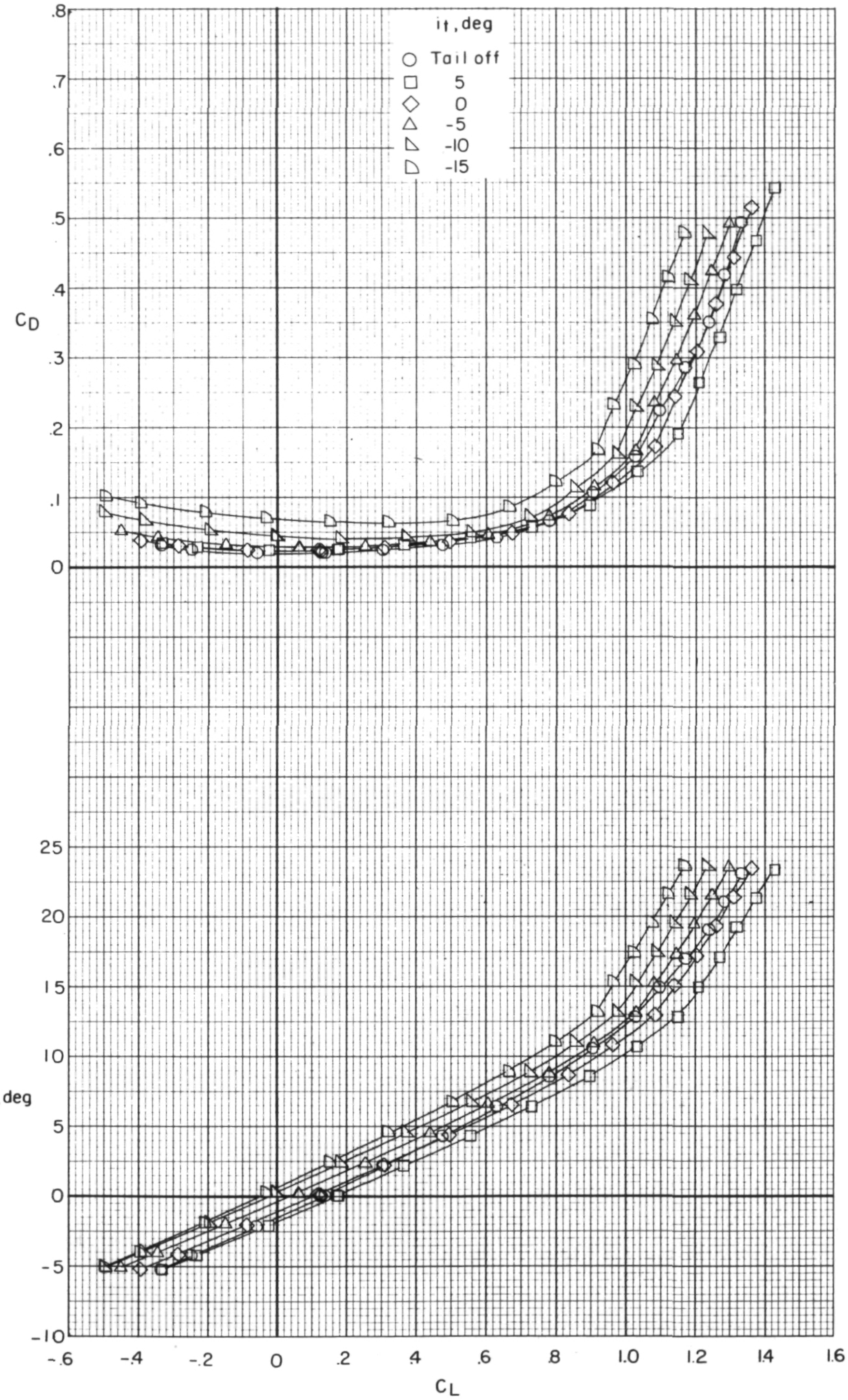

Figure 6.- Effect of horizontal-tail deflection on longitudinal aerodynamic characteristics. Nacelles removed; mid tail; $WFVH_2$.

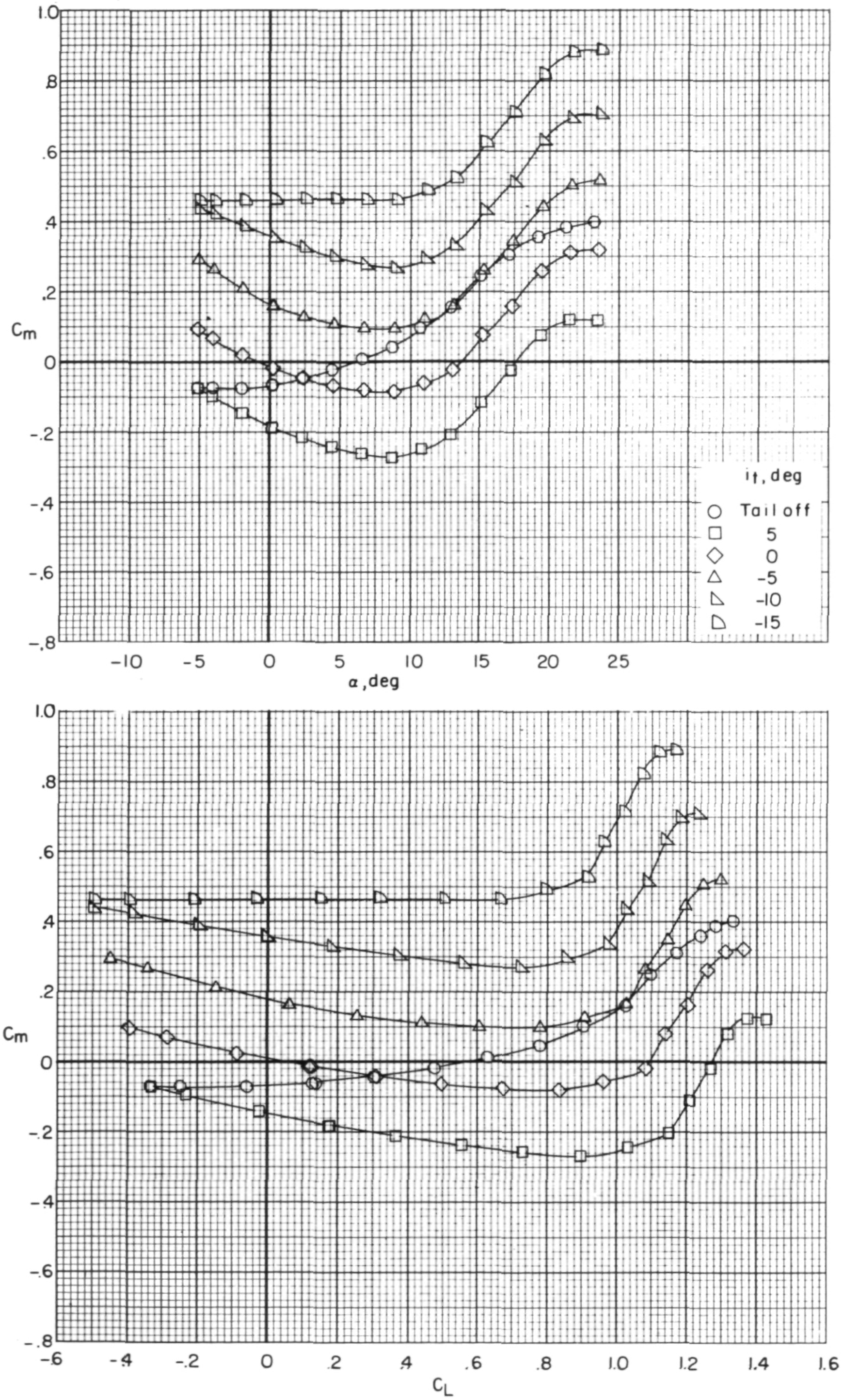

Figure 6.- Concluded.

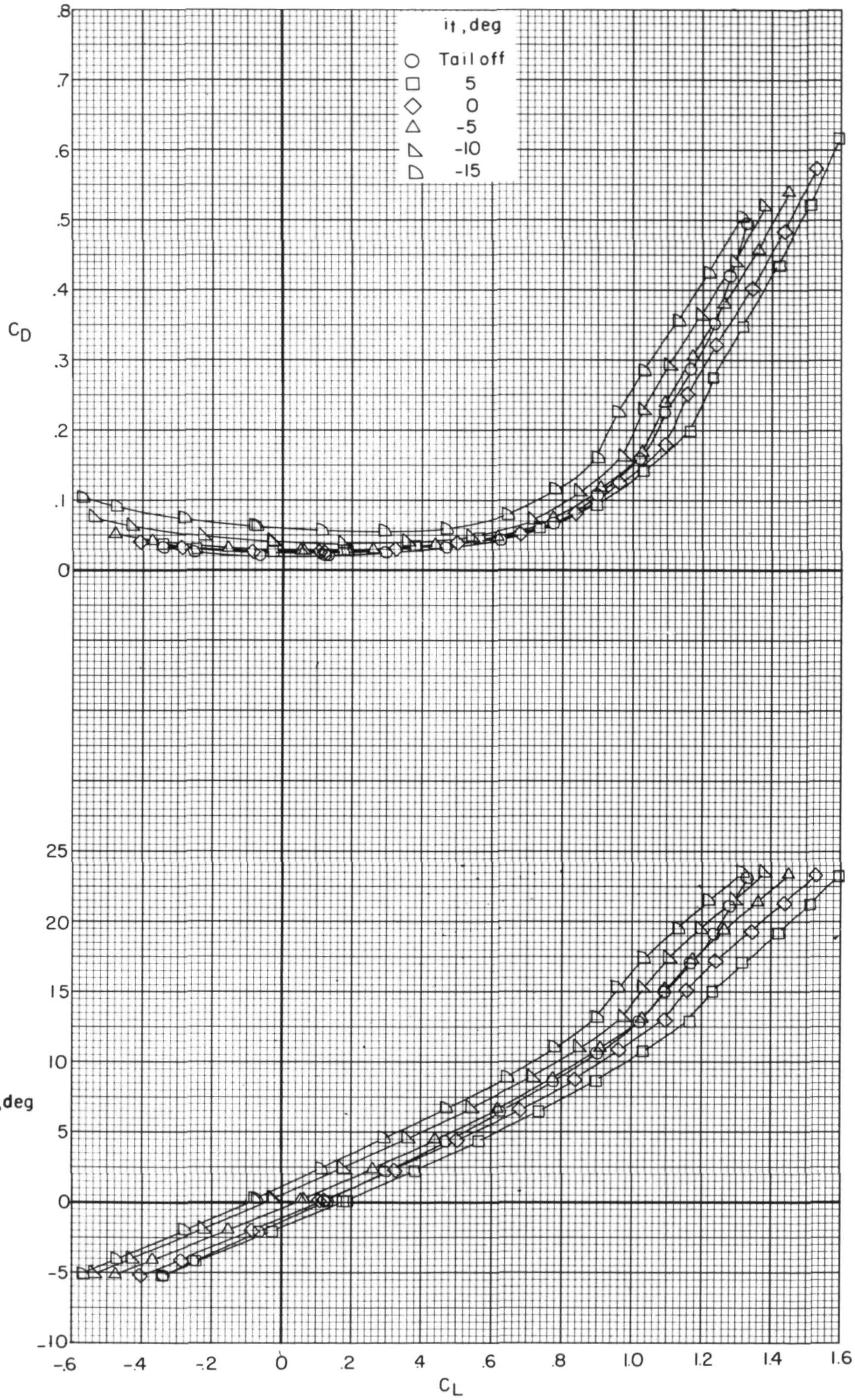

Figure 7.- Effect of horizontal-tail deflection on longitudinal aerodynamic characteristics. Nacelles removed; low tail; $WFVH_3$.

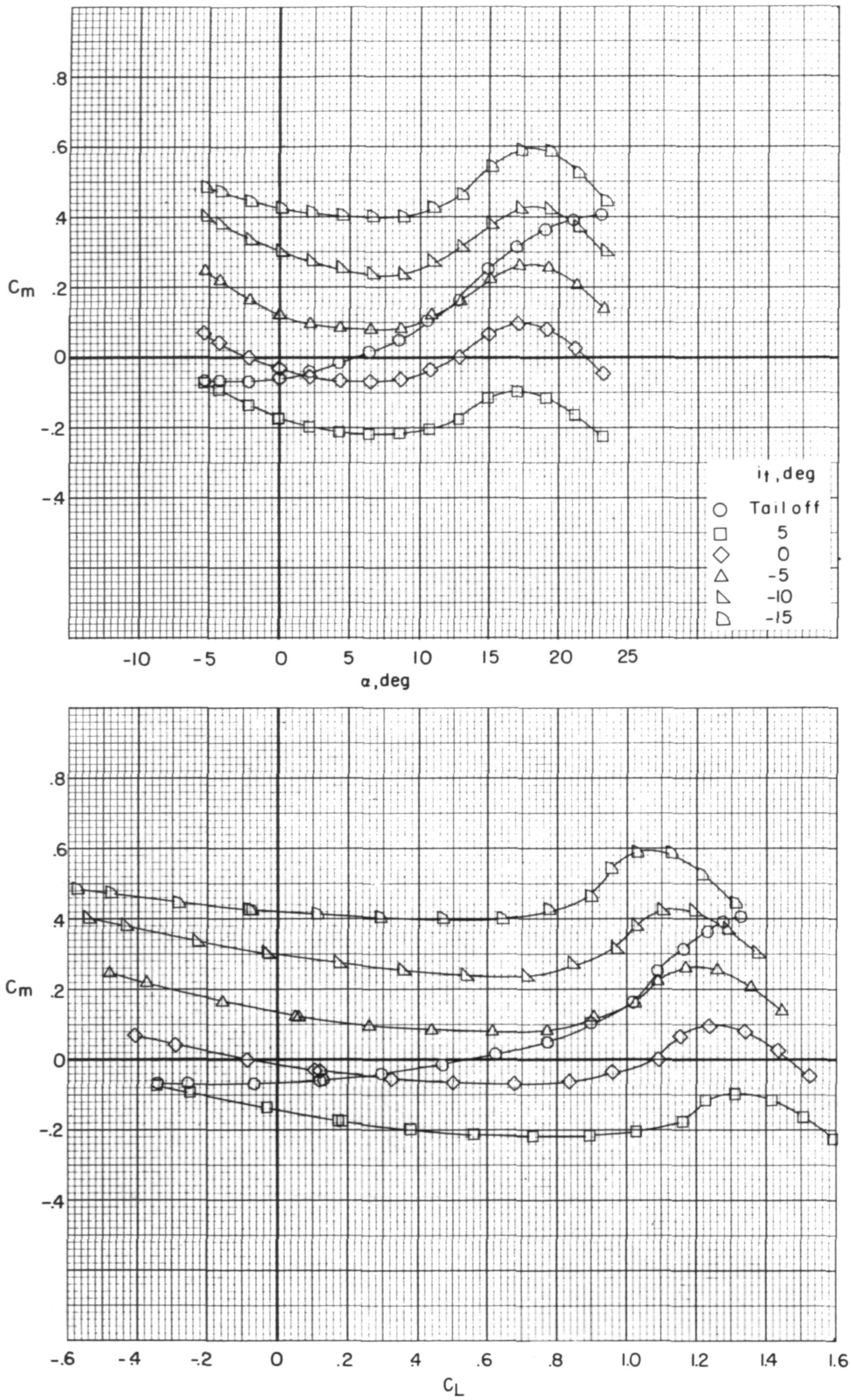

Figure 7.- Concluded.

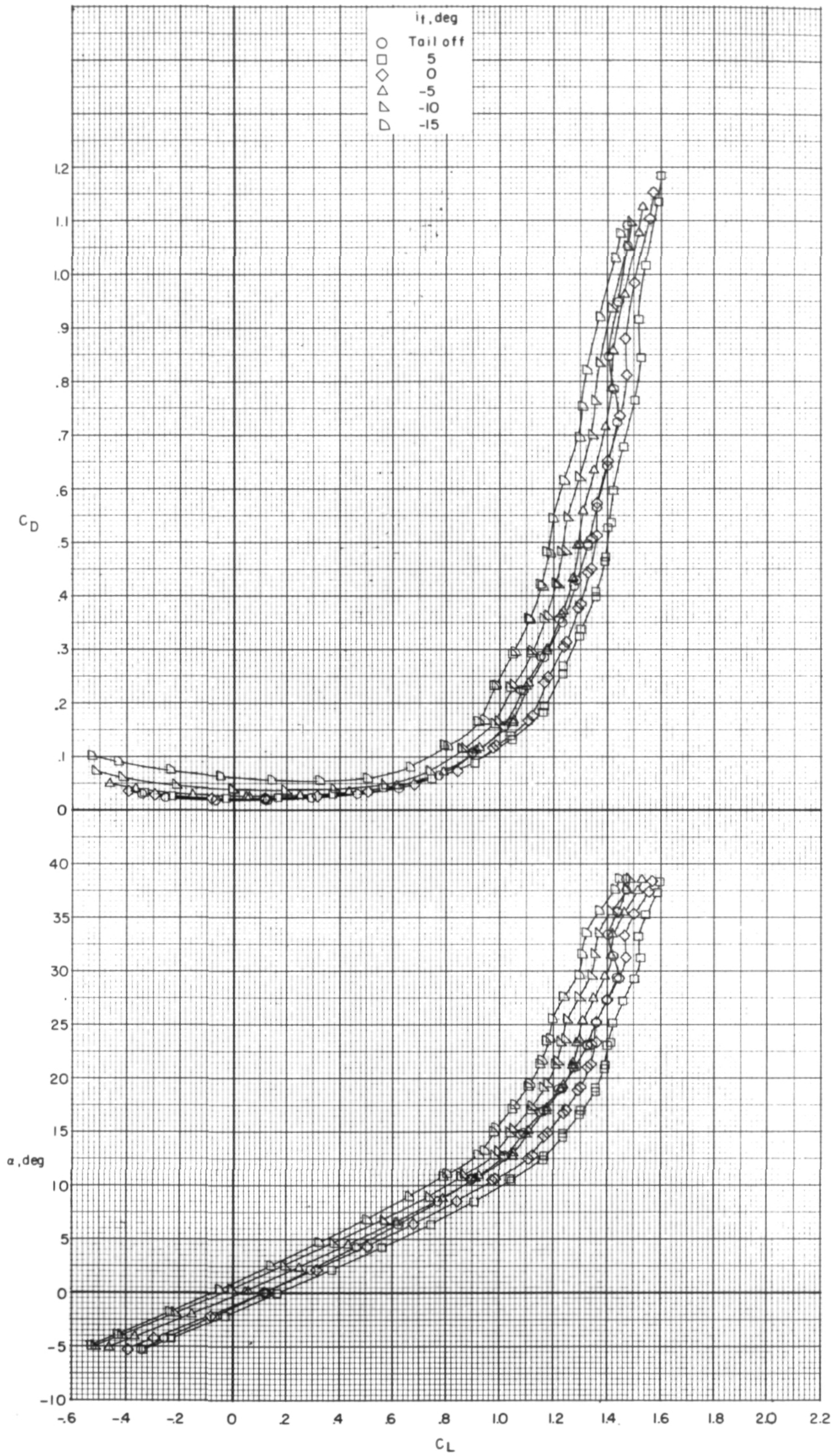

Figure 8.- Effect of horizontal-tail deflection on longitudinal aerodynamic characteristics. Nacelles removed; high tail; $WFVH_1$; complete α range.

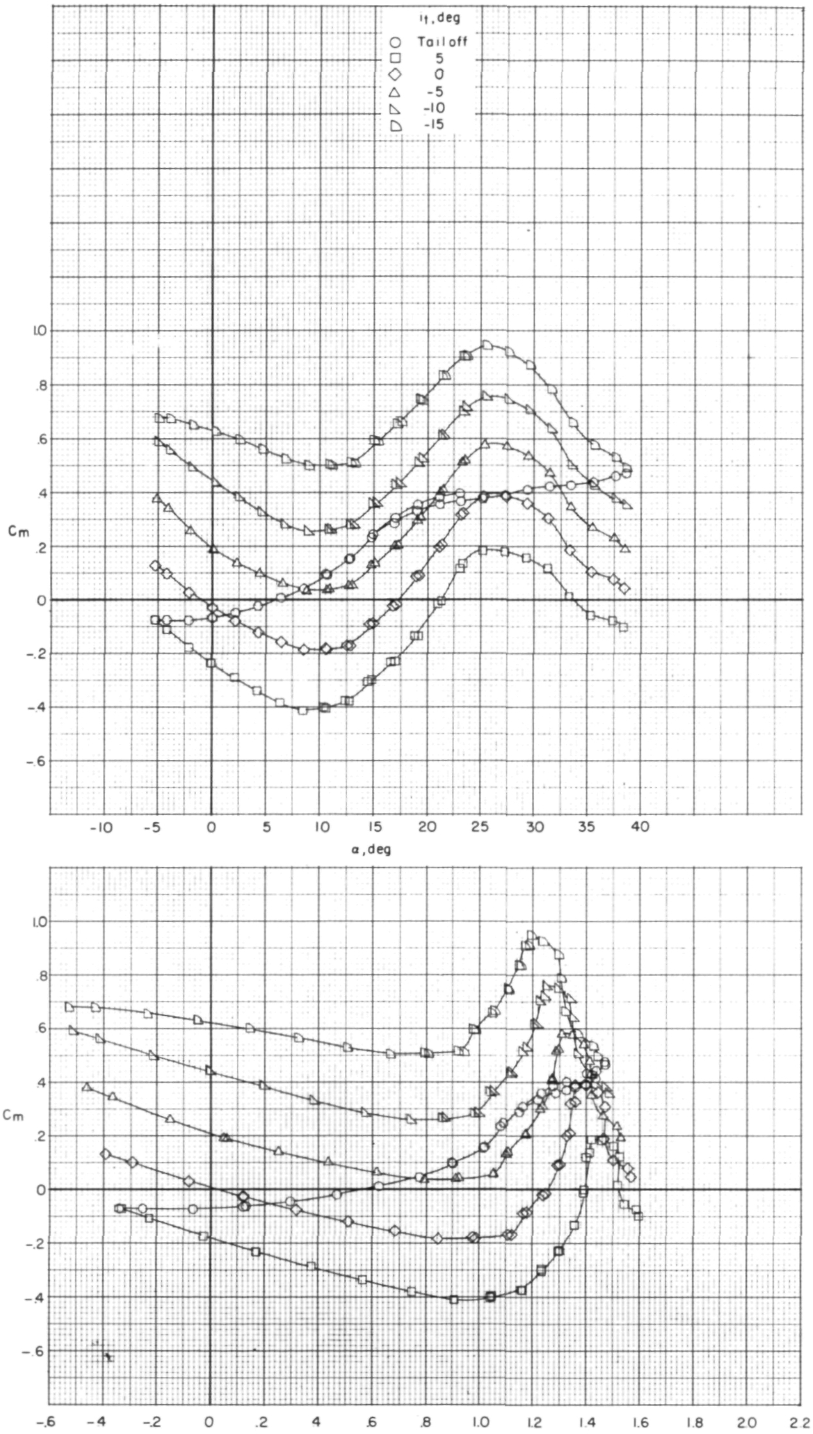

Figure 8.- Concluded.

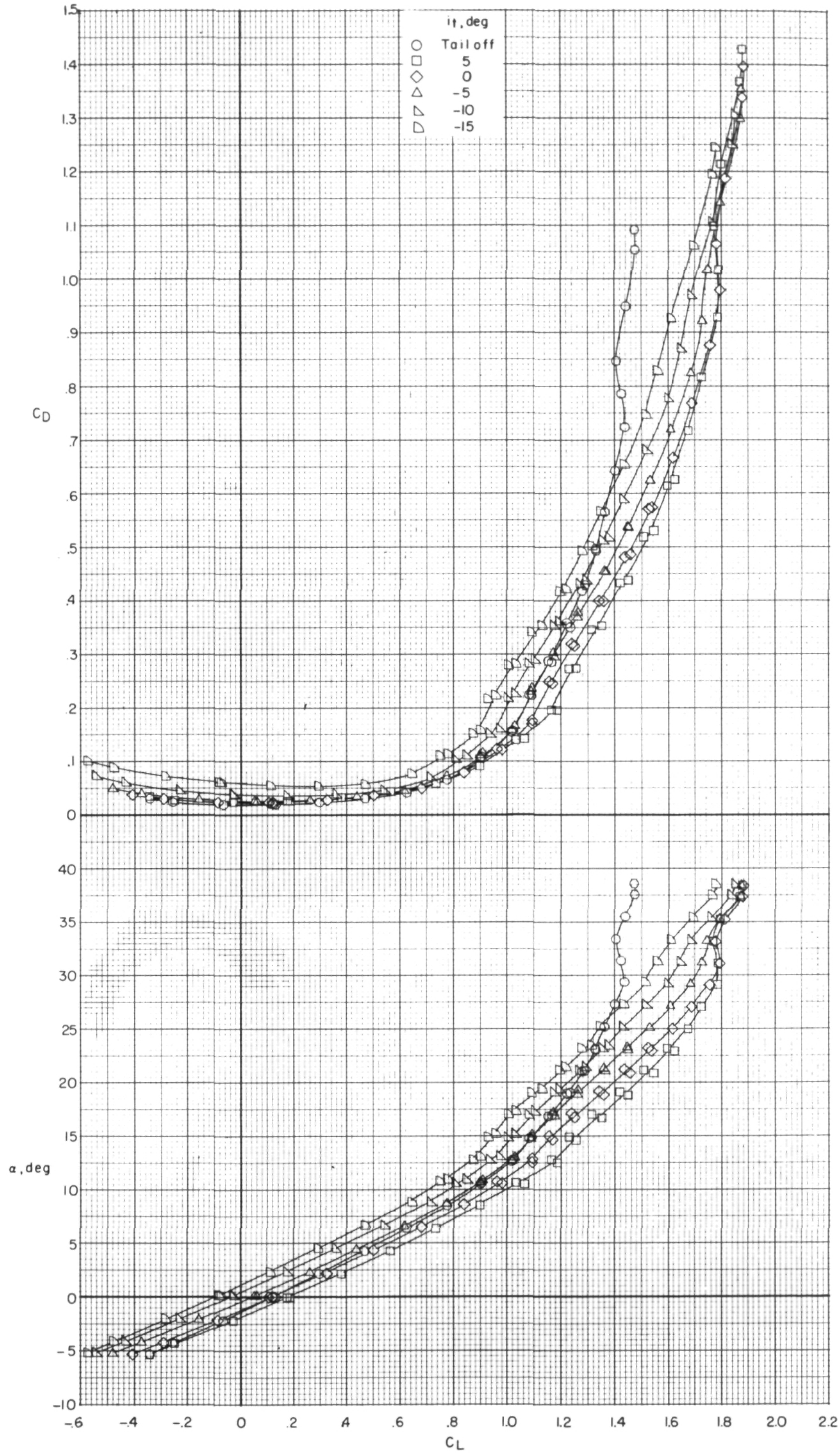

Figure 9.- Effect of horizontal-tail deflection on longitudinal aerodynamic characteristics. Nacelles removed; low tail; WFVH$_3$; complete α range.

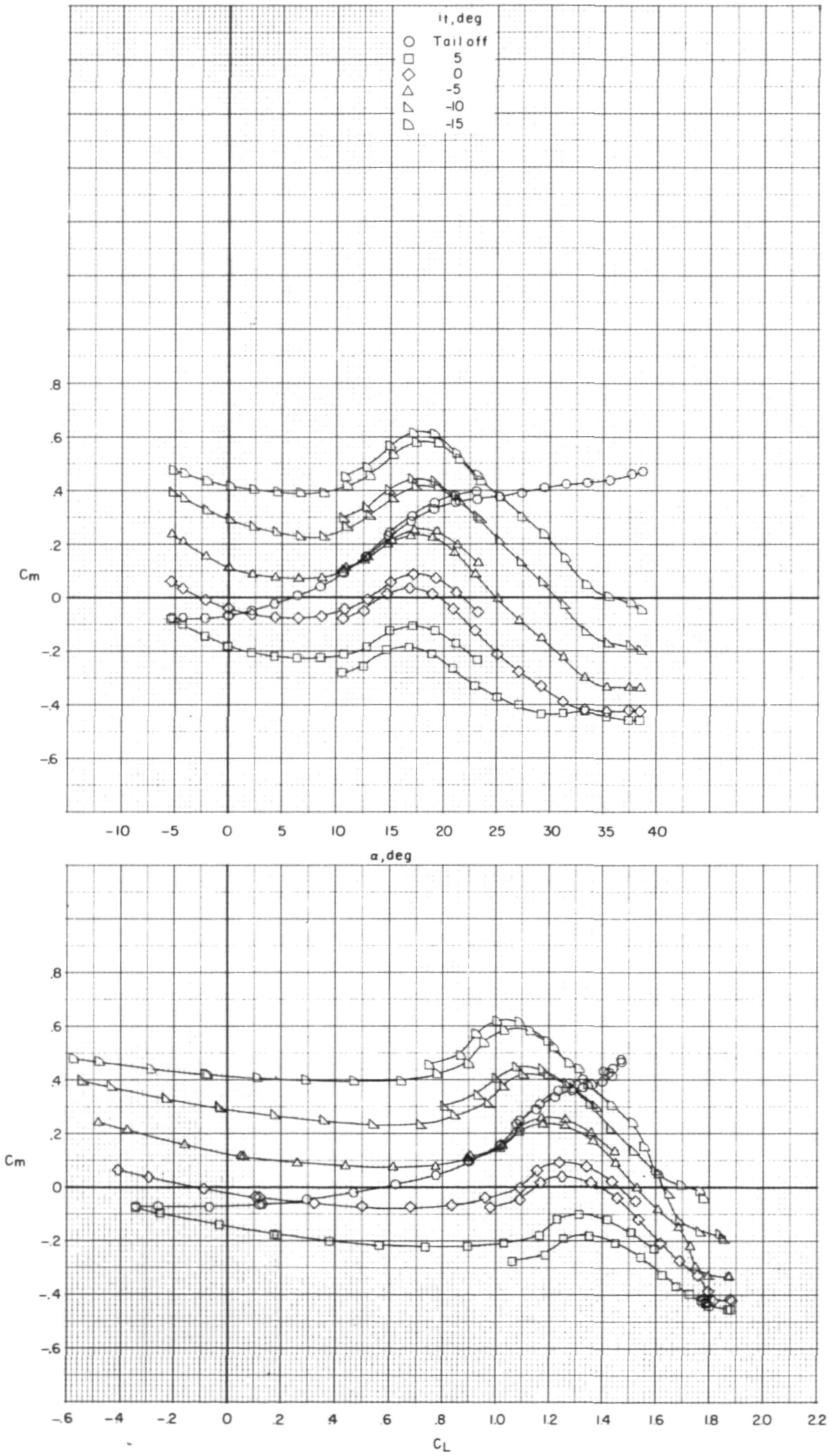

Figure 9.- Concluded.

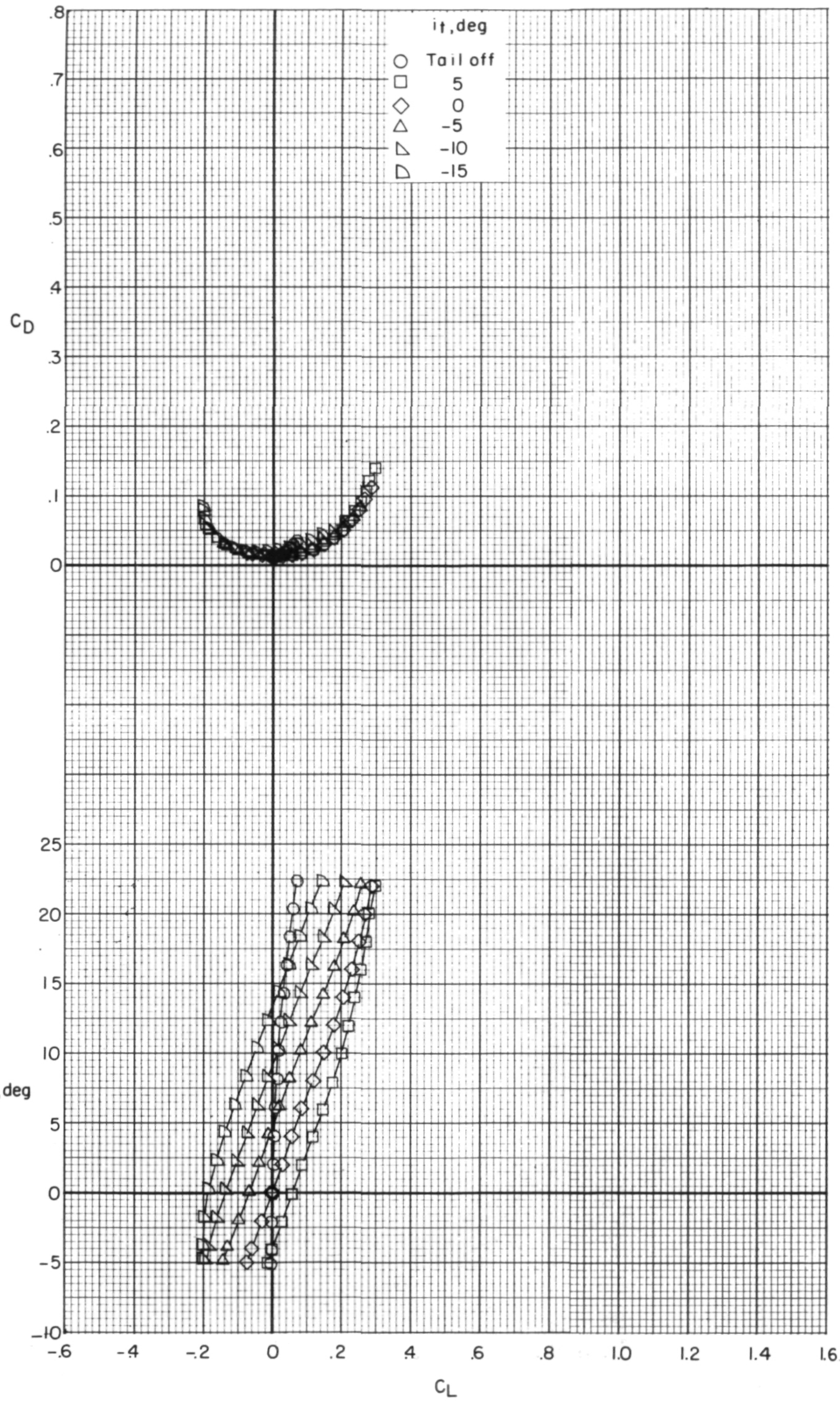

Figure 10.- Effect of horizontal-tail deflection on longitudinal aerodynamic characteristics. Wing and nacelles removed; high tail; FVH_1.

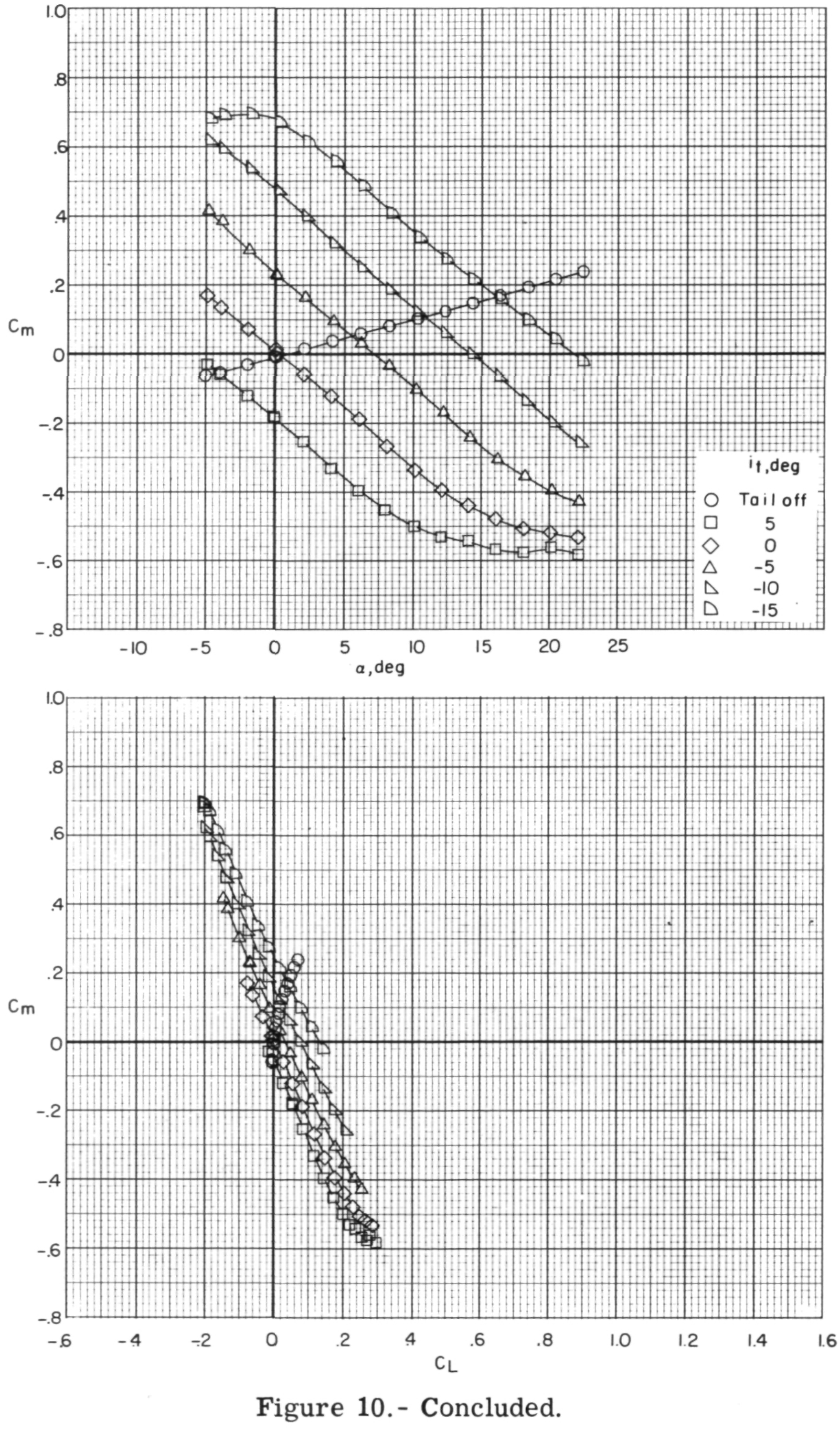

Figure 10.- Concluded.

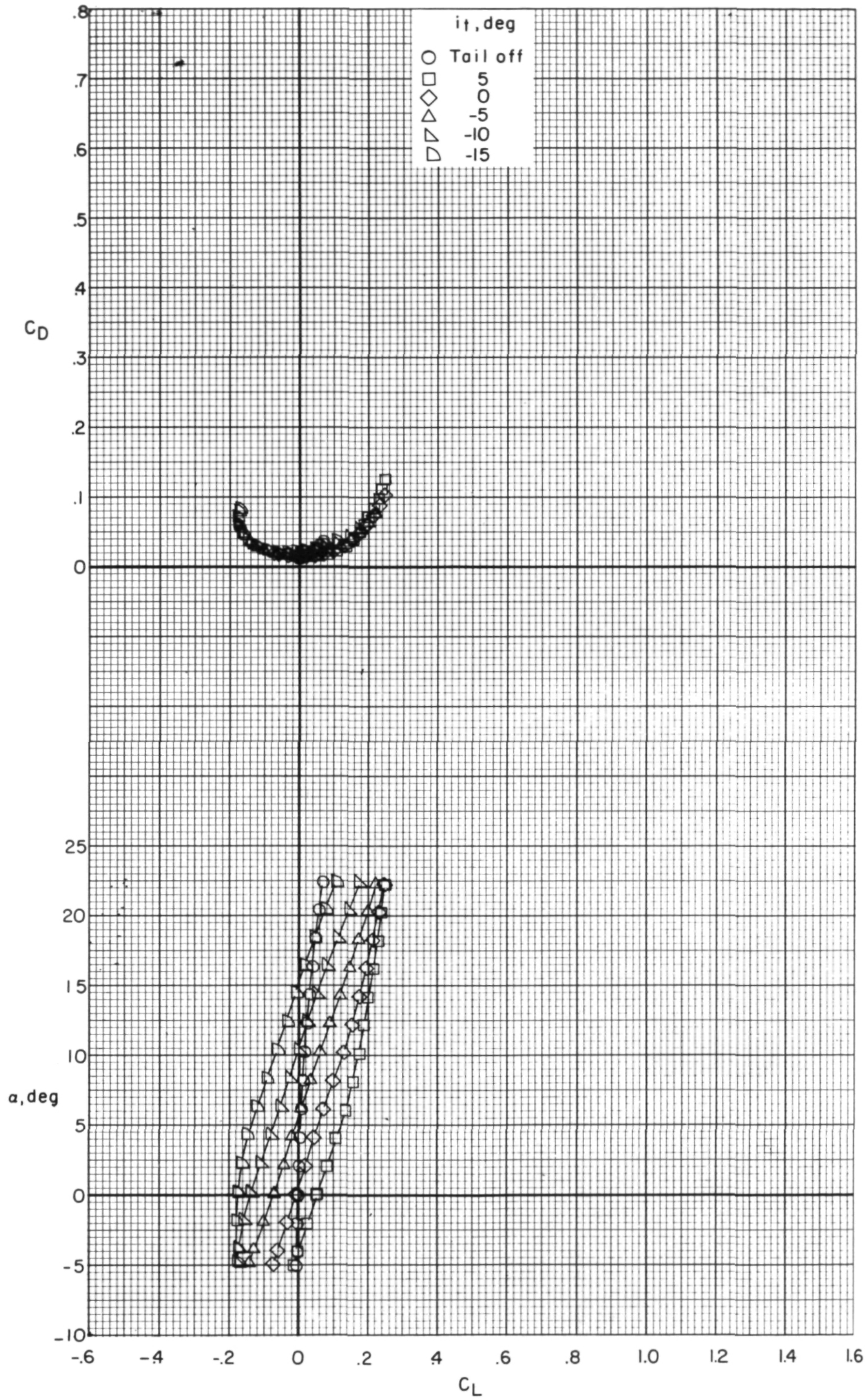

Figure 11.- Effect of horizontal-tail deflection on longitudinal aerodynamic characteristics. Wing and nacelles removed; mid tail; FVH_2.

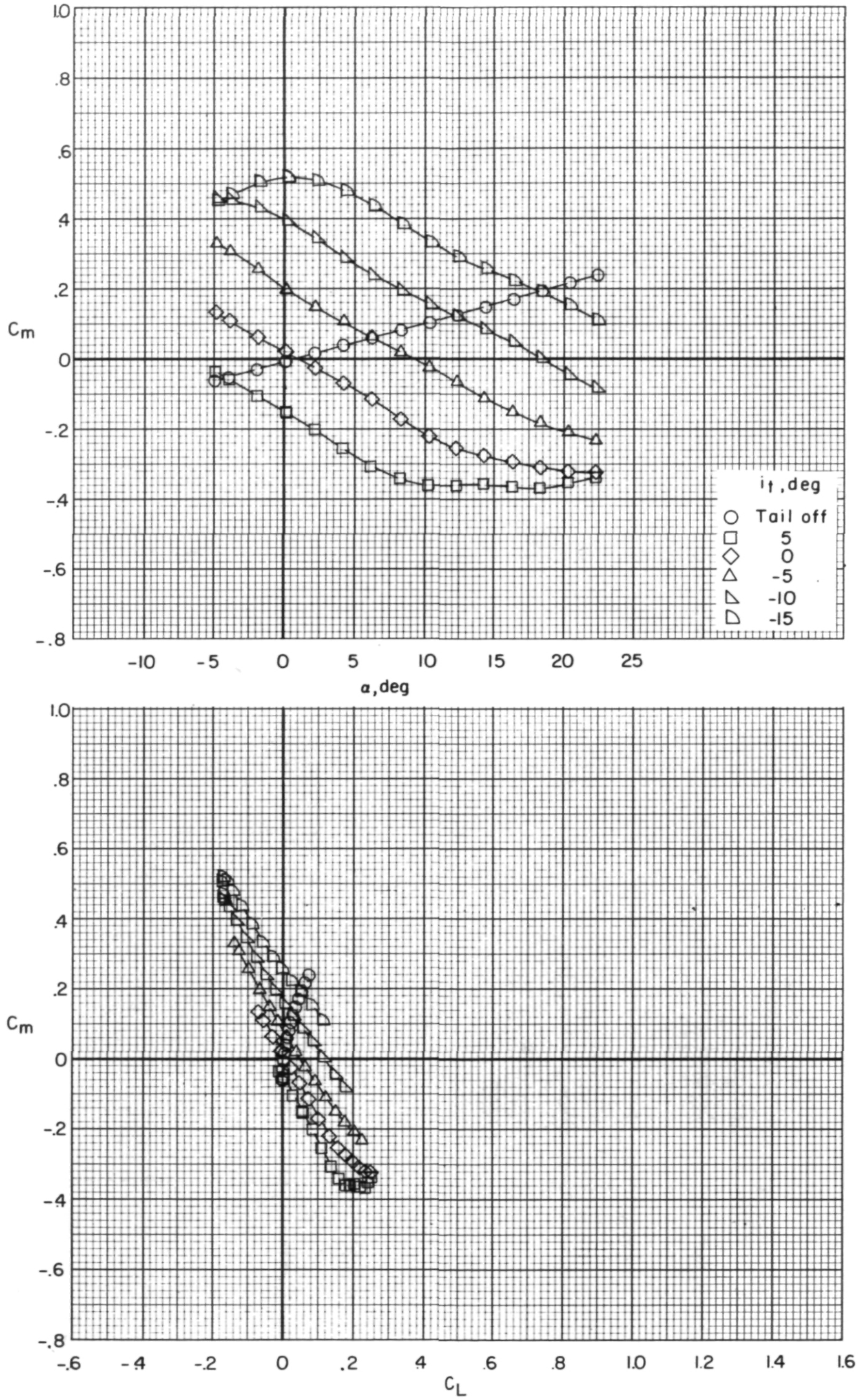

Figure 11.- Concluded.

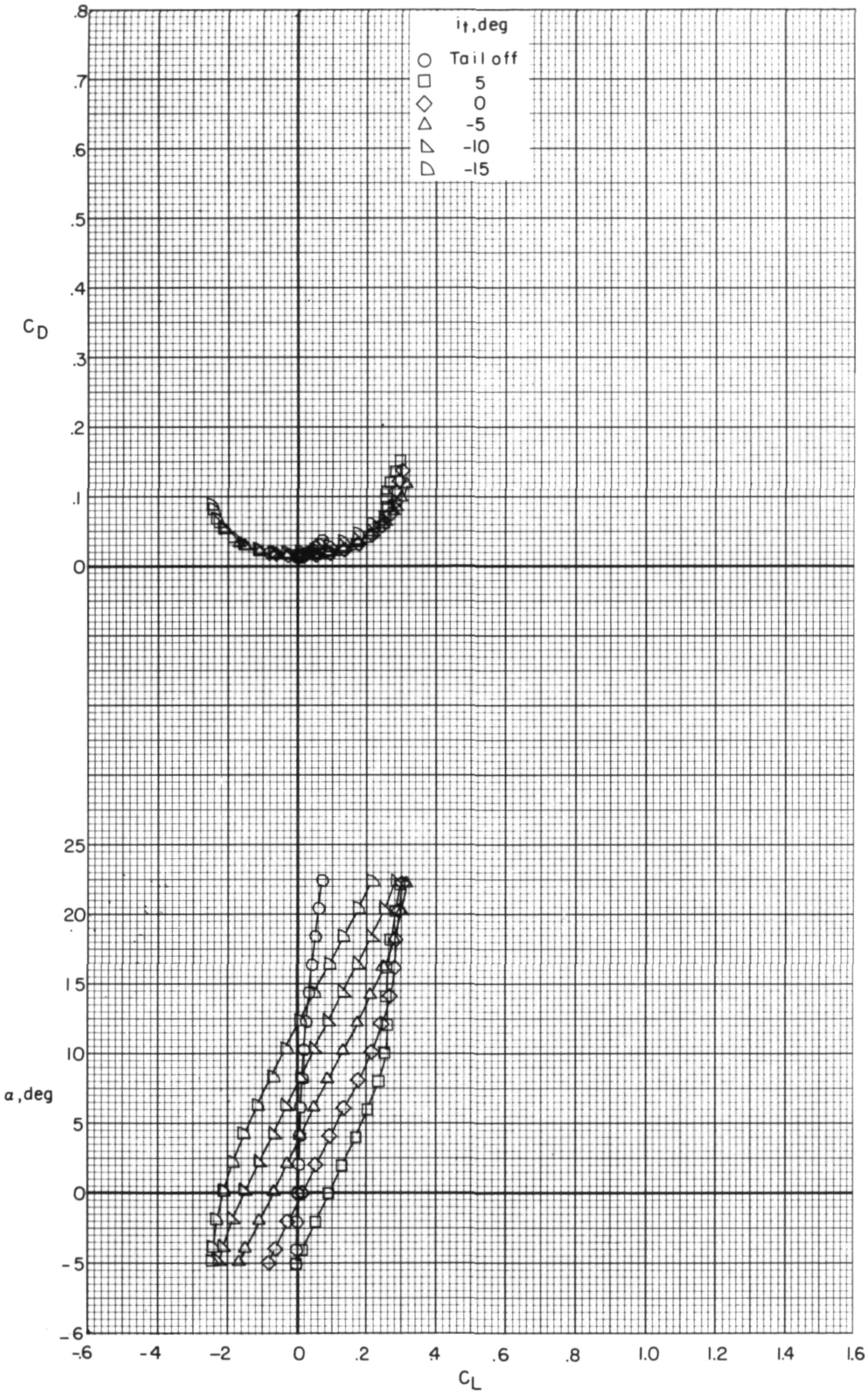

Figure 12.- Effect of horizontal-tail deflection on longitudinal aerodynamic characteristics. Wing and nacelles removed; low tail; FVH_3.

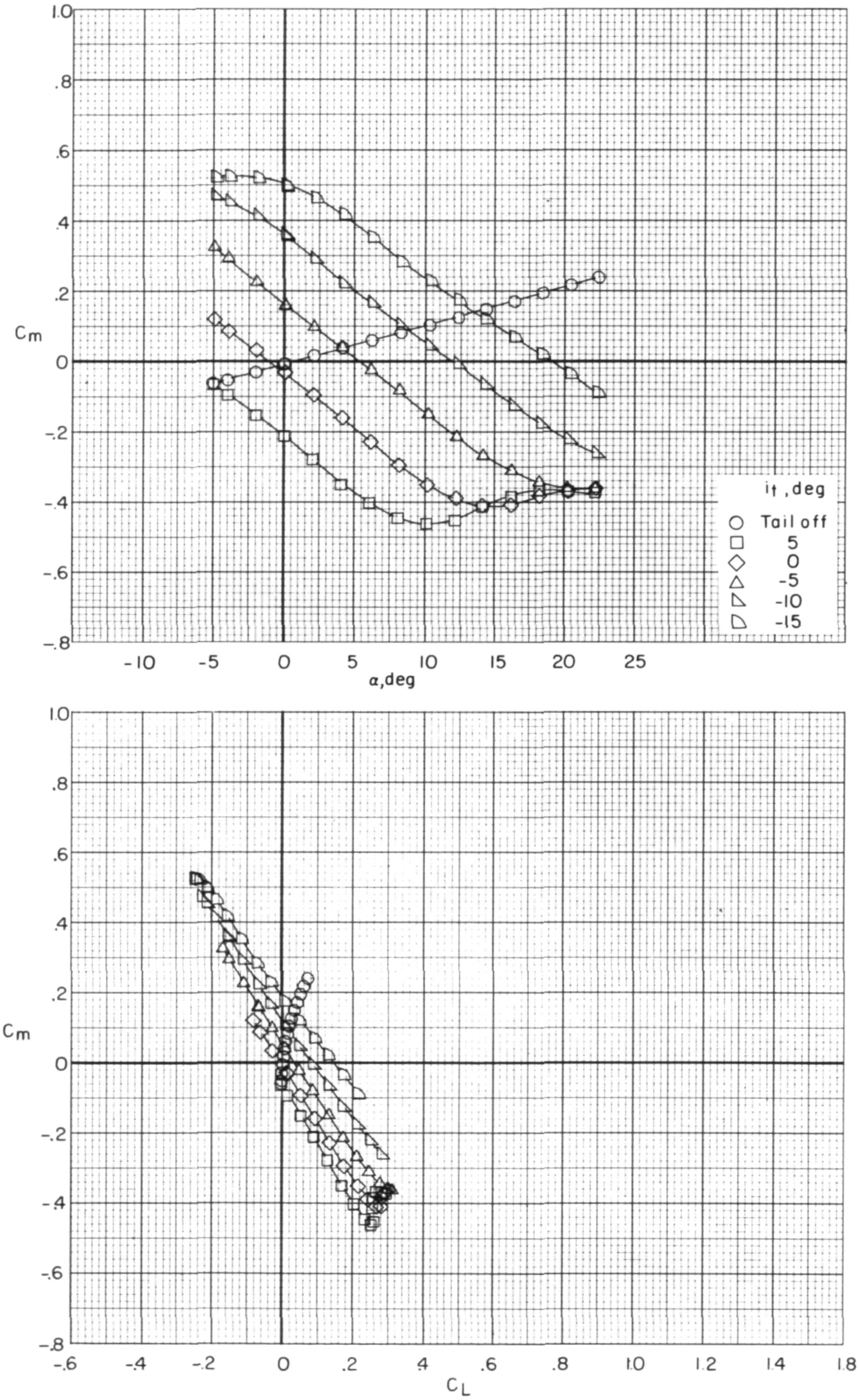

Figure 12.- Concluded.

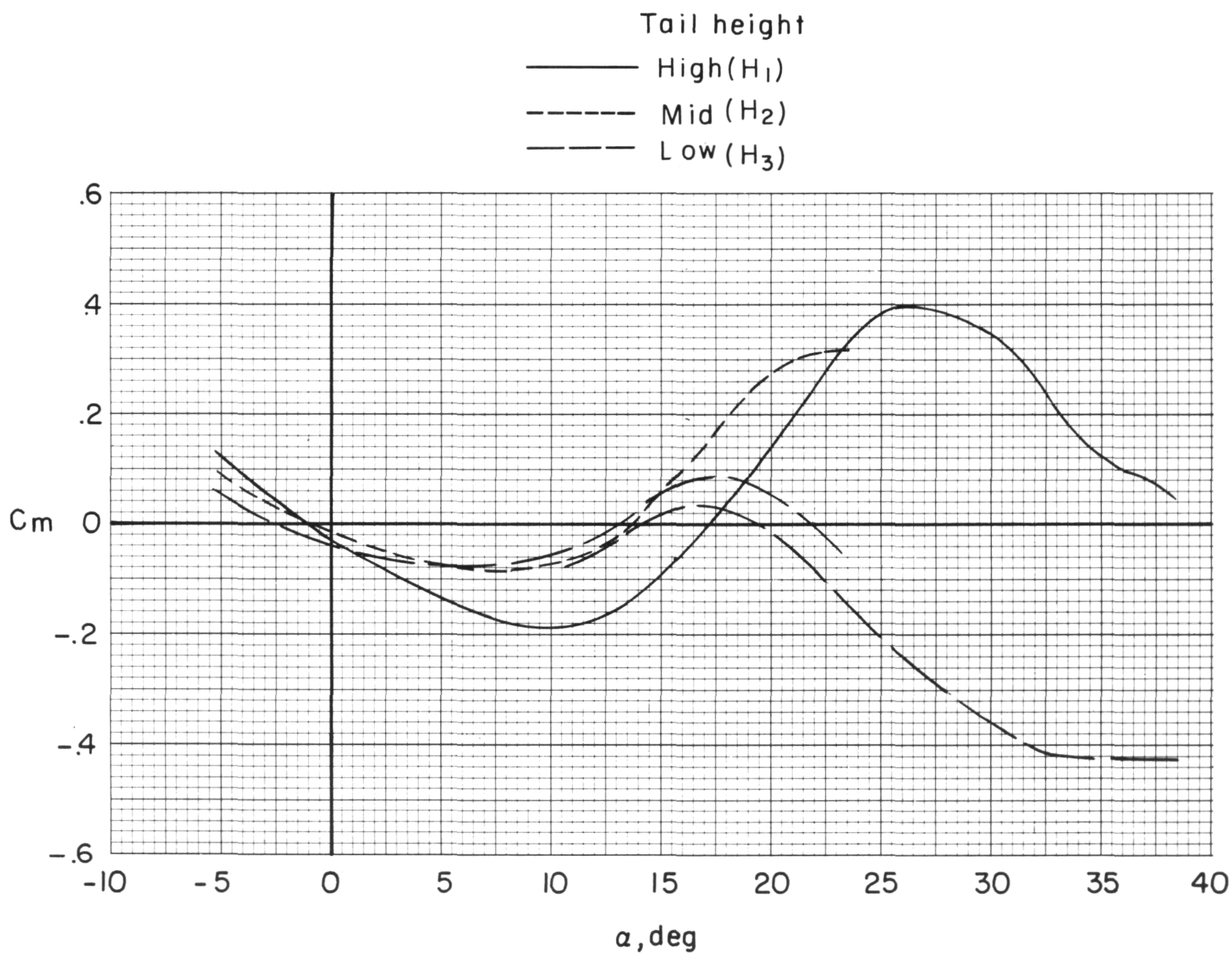

Figure 13.- Effect of tail configuration on pitching-moment characteristics for model without nacelles $i_t = 0^o$.

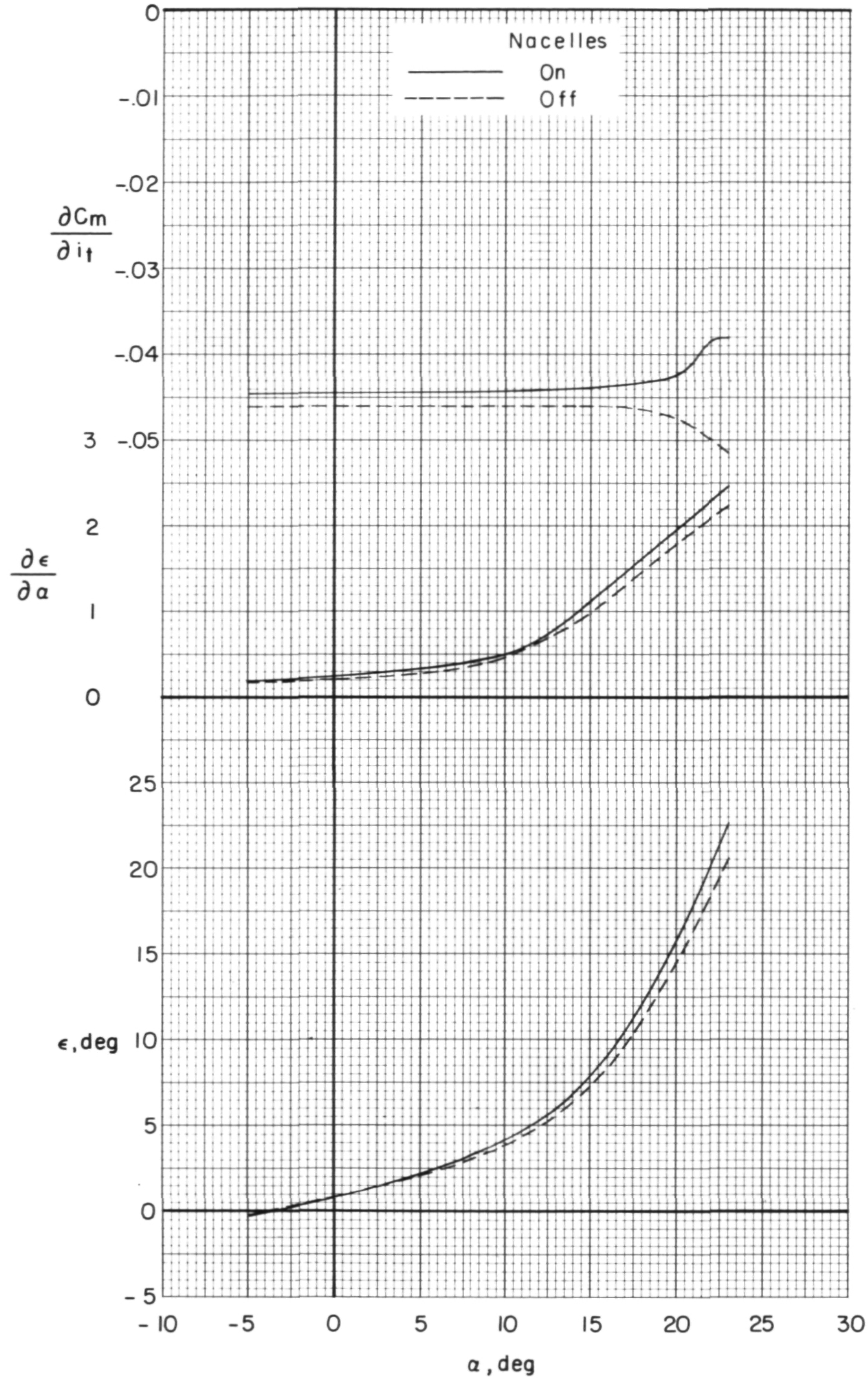

Figure 14.- Effect of nacelles on effective downwash angle, downwash gradient, and stabilizer effectiveness for model with high tail.

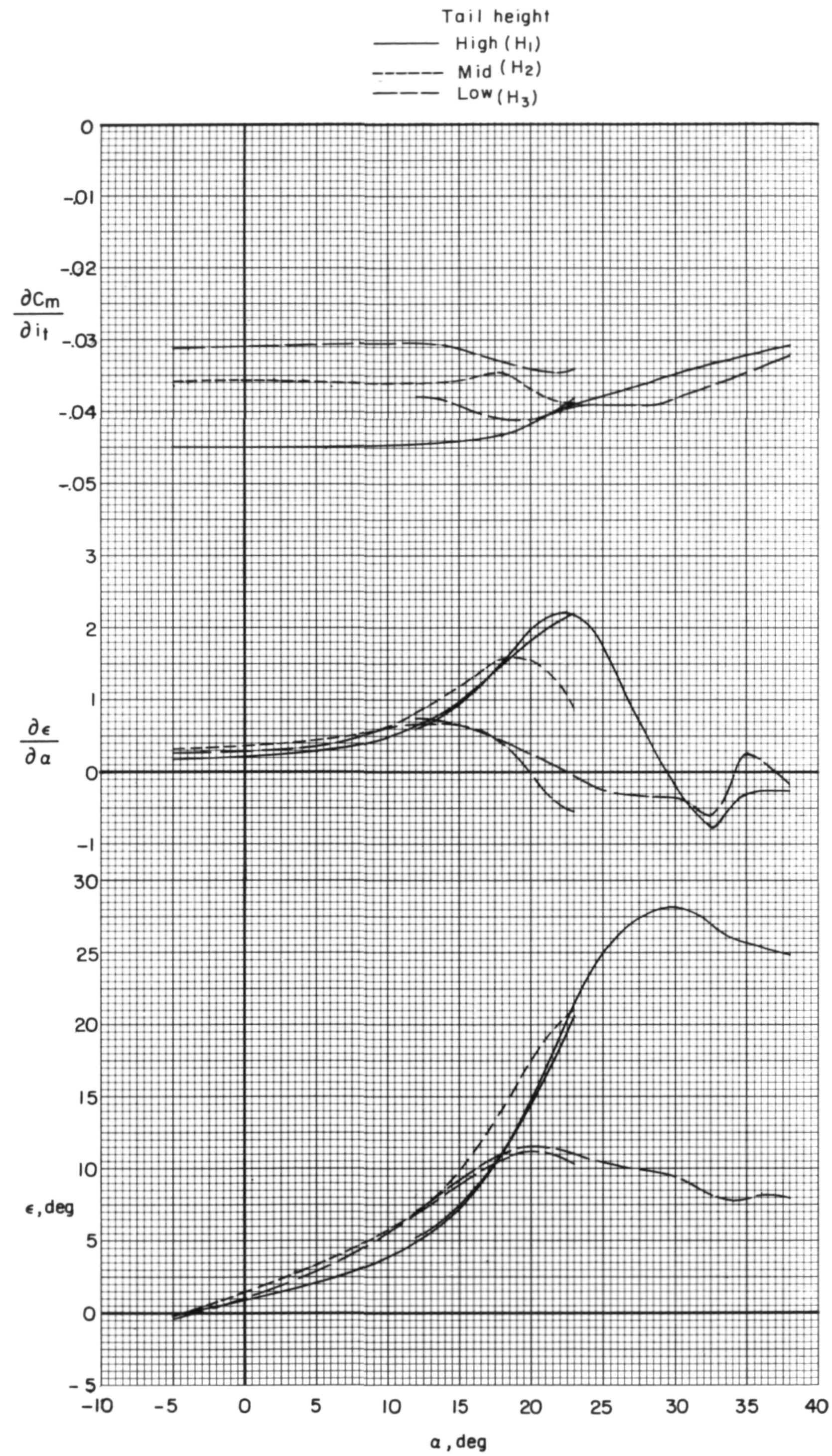

Figure 15.- Effect of tail height on effective downwash angle, downwash gradient, and stabilizer effectiveness for model without nacelles.

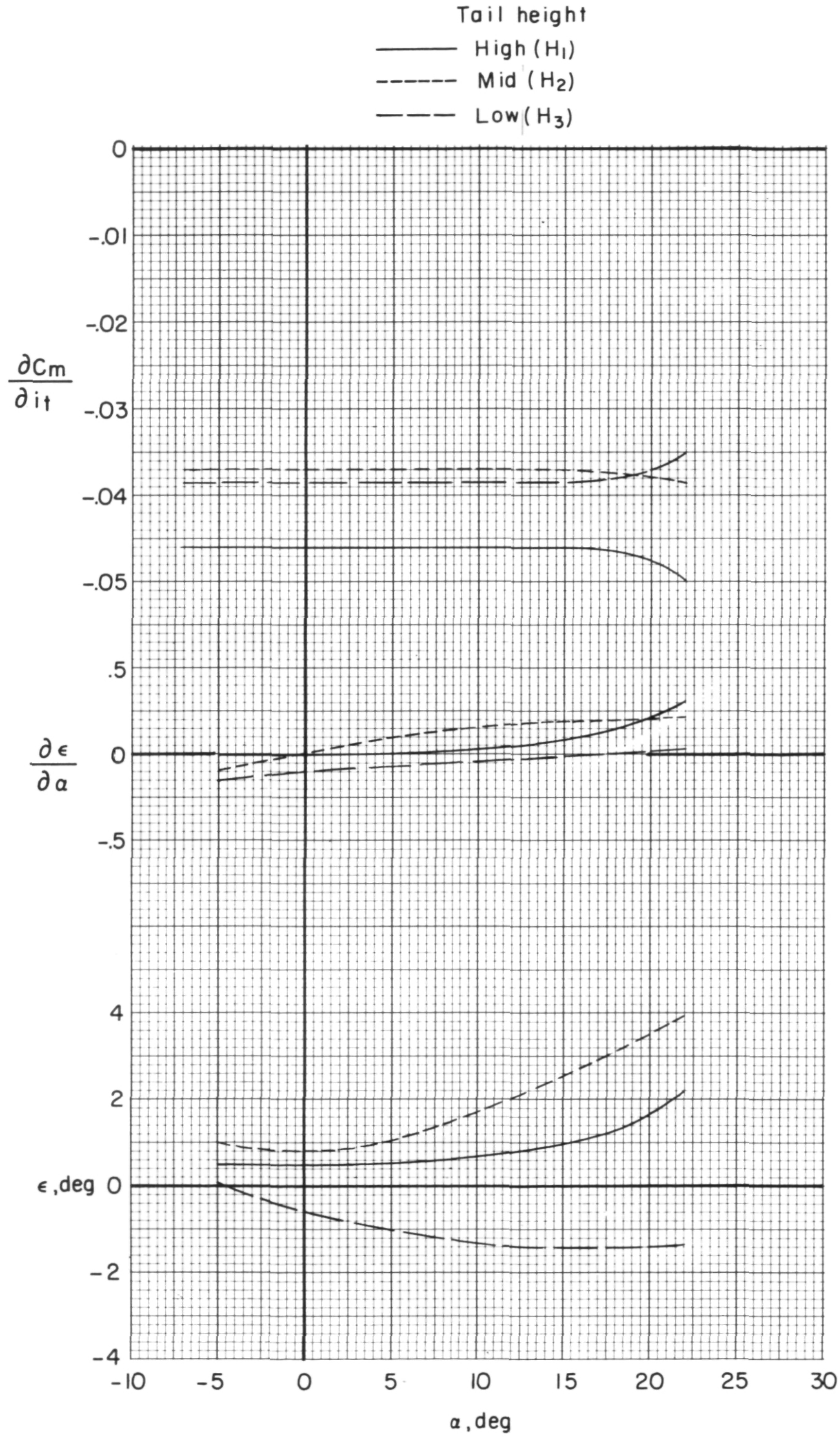

Figure 16.- Effect of tail height on effective downwash angle, downwash gradient, and stabilizer effectiveness for wing-off model without nacelles.

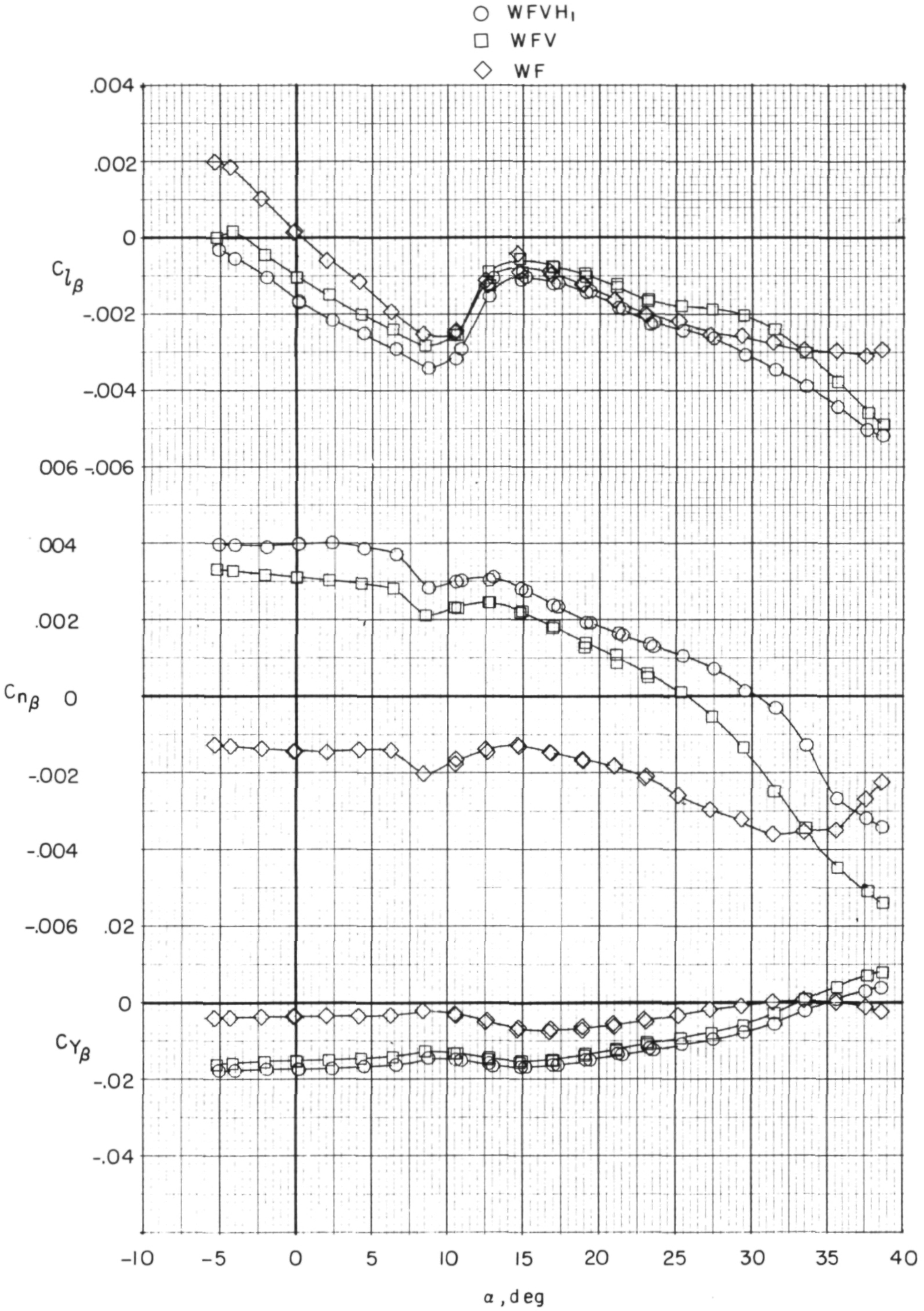

Figure 17.- Effect of horizontal and vertical tails on static lateral-stability derivatives. Nacelles removed; high tail; $i_t = -5^{\circ}$; complete α range.

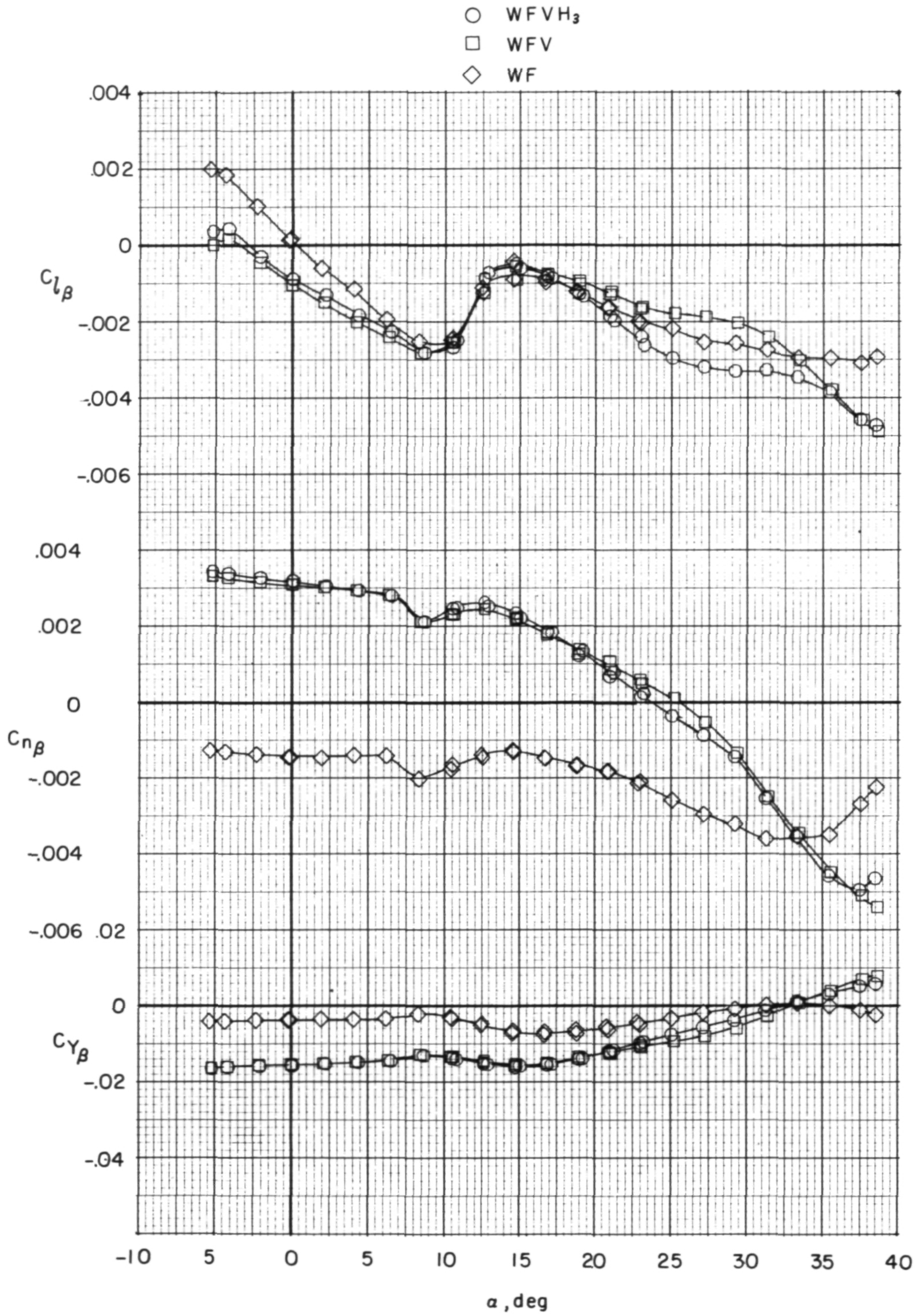

Figure 18.- Effect of horizontal and vertical tails on static lateral-stability derivatives. Nacelles removed; low tail; $i_t = -5^{\circ}$; complete α range.

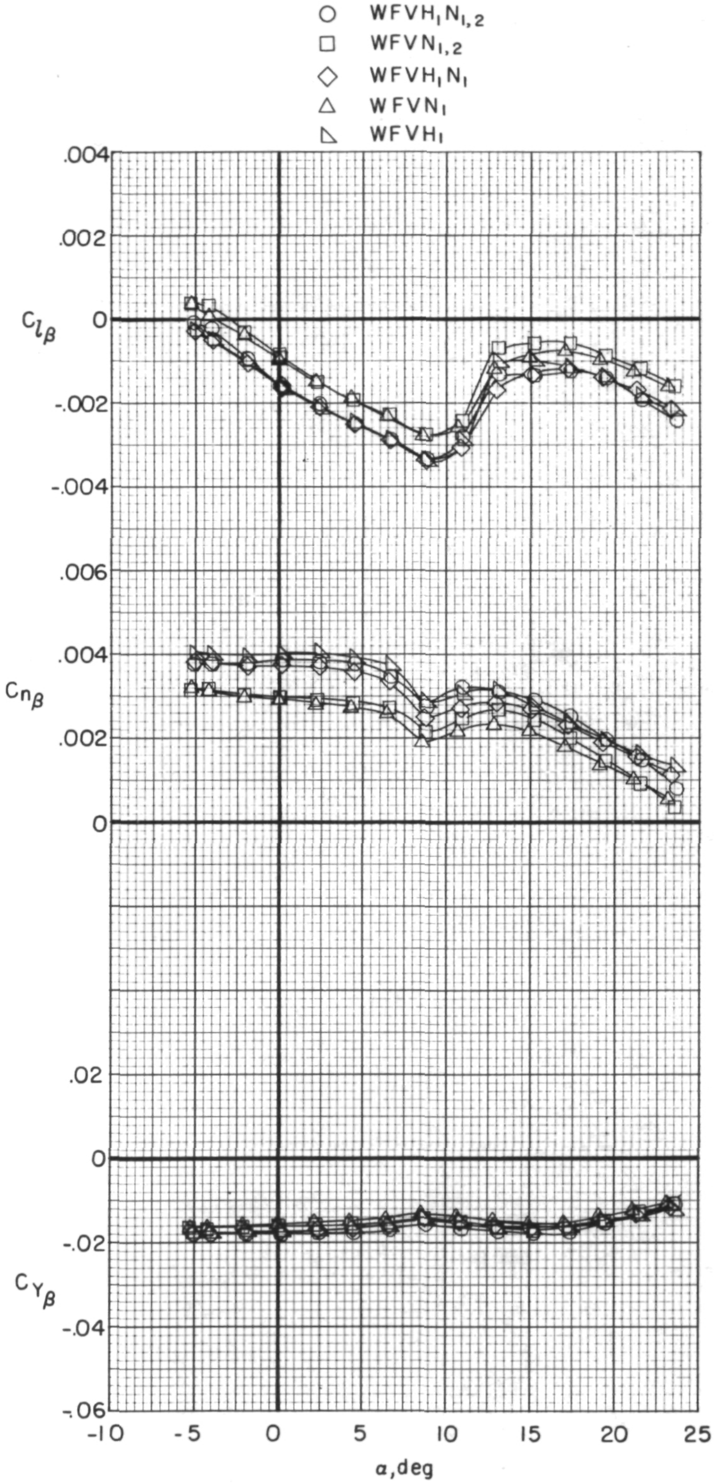

Figure 19.- Effect of horizontal tail and nacelles on static lateral-stability derivatives. High tail; $i_t = -5^\circ$.

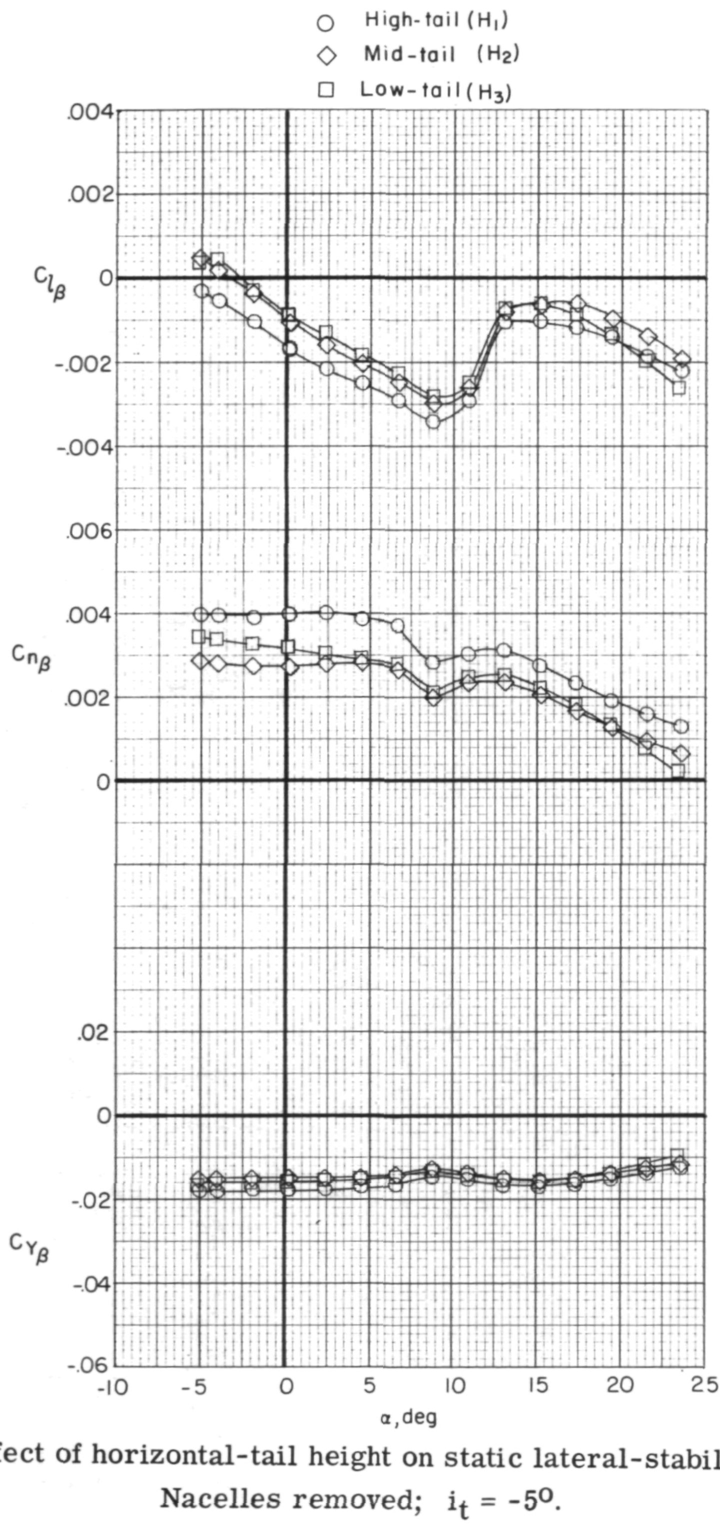

Figure 20.- Effect of horizontal-tail height on static lateral-stability derivatives. Nacelles removed; $i_t = -5^{\circ}$.

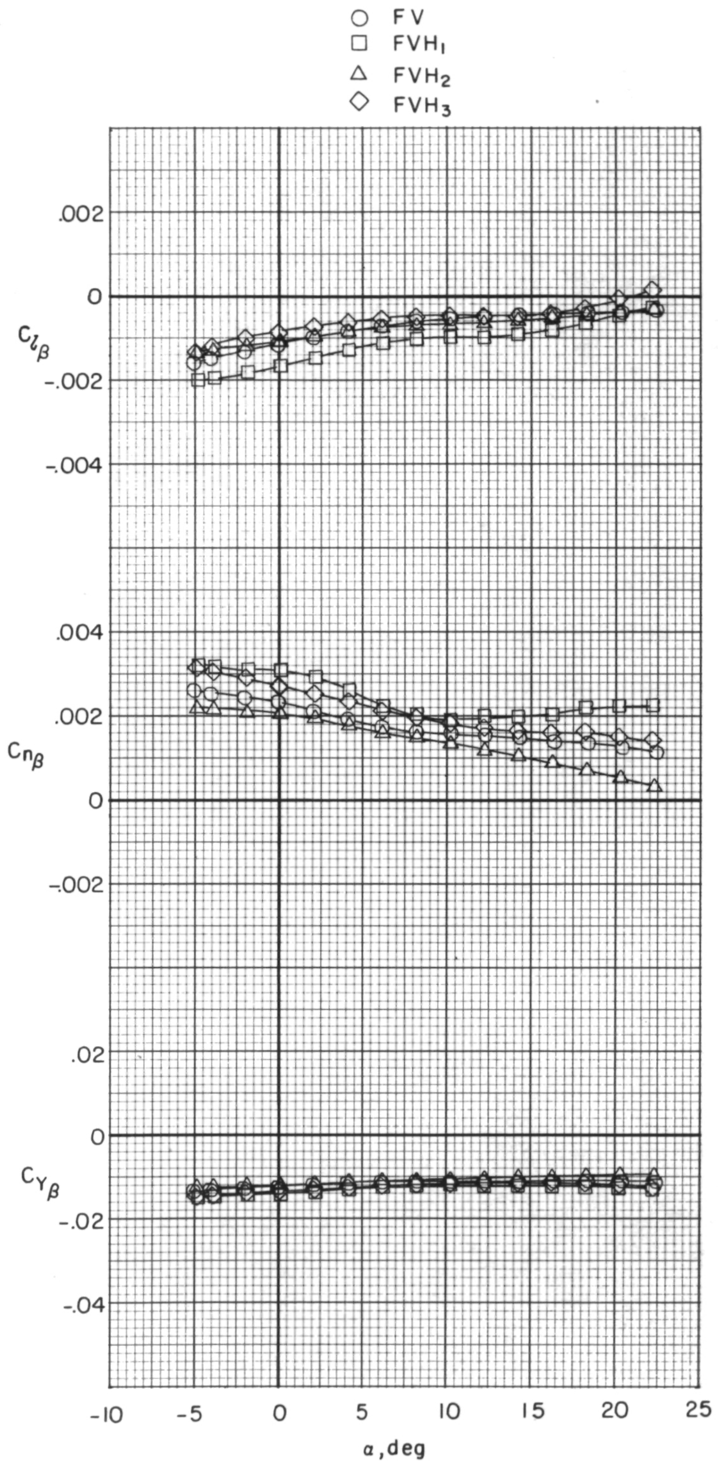

Figure 21.- Effect of horizontal-tail height on static lateral-stability derivatives. Wing and nacelles removed; $i_t = -5^{\circ}$.

"The aeronautical and space activities of the United States shall be conducted so as to contribute . . . to the expansion of human knowledge of phenomena in the atmosphere and space. The Administration shall provide for the widest practicable and appropriate dissemination of information concerning its activities and the results thereof."

—NATIONAL AERONAUTICS AND SPACE ACT OF 1958

NASA SCIENTIFIC AND TECHNICAL PUBLICATIONS

TECHNICAL REPORTS: Scientific and technical information considered important, complete, and a lasting contribution to existing knowledge.

TECHNICAL NOTES: Information less broad in scope but nevertheless of importance as a contribution to existing knowledge.

TECHNICAL MEMORANDUMS: Information receiving limited distribution because of preliminary data, security classification, or other reasons. Also includes conference proceedings with either limited or unlimited distribution.

CONTRACTOR REPORTS: Scientific and technical information generated under a NASA contract or grant and considered an important contribution to existing knowledge.

TECHNICAL TRANSLATIONS: Information published in a foreign language considered to merit NASA distribution in English.

SPECIAL PUBLICATIONS: Information derived from or of value to NASA activities. Publications include final reports of major projects, monographs, data compilations, handbooks, sourcebooks, and special bibliographies.

TECHNOLOGY UTILIZATION PUBLICATIONS: Information on technology used by NASA that may be of particular interest in commercial and other non-aerospace applications. Publications include Tech Briefs, Technology Utilization Reports and Technology Surveys.

Details on the availability of these publications may be obtained from:

SCIENTIFIC AND TECHNICAL INFORMATION OFFICE

NATIONAL AERONAUTICS AND SPACE ADMINISTRATION

Washington, D.C. 20546